Measuring Fatigue Damage in Materials--Phase I

WARNING:
Please read the Export Control and License Agreement on the back cover before removing the Wrapping Material.

Technical Report

Measuring Fatigue Damage in Materials—Phase I

TR-110250

Final Report
March 1998

Prepared for
EPRI
3412 Hillview Avenue
Palo Alto, CA 94304

EPRI Project Manager
Stan T. Rosinski

DISCLAIMER OF WARRANTIES AND LIMITATION OF LIABILITIES

THIS REPORT WAS PREPARED BY THE ORGANIZATION(S) NAMED BELOW AS AN ACCOUNT OF WORK SPONSORED OR COSPONSORED BY THE ELECTRIC POWER RESEARCH INSTITUTE, INC. (EPRI). NEITHER EPRI, ANY MEMBER OF EPRI, ANY COSPONSOR, THE ORGANIZATION(S) BELOW, NOR ANY PERSON ACTING ON BEHALF OF ANY OF THEM:

A) MAKES ANY WARRANTY OR REPRESENTATION WHATSOEVER, EXPRESS OR IMPLIED, (I) WITH RESPECT TO THE USE OF ANY INFORMATION, APPARATUS, METHOD, PROCESS, OR SIMILAR ITEM DISCLOSED IN THIS REPORT, INCLUDING MERCHANTABILITY AND FITNESS FOR A PARTICULAR PURPOSE, OR (II) THAT SUCH USE DOES NOT INFRINGE ON OR INTERFERE WITH PRIVATELY OWNED RIGHTS, INCLUDING ANY PARTY'S INTELLECTUAL PROPERTY, OR (III) THAT THIS REPORT IS SUITABLE TO ANY PARTICULAR USER'S CIRCUMSTANCE; OR

(B) ASSUMES RESPONSIBILITY FOR ANY DAMAGES OR OTHER LIABILITY WHATSOEVER (INCLUDING ANY CONSEQUENTIAL DAMAGES, EVEN IF EPRI OR ANY EPRI REPRESENTATIVE HAS BEEN ADVISED OF THE POSSIBILITY OF SUCH DAMAGES) RESULTING FROM YOUR SELECTION OR USE OF THIS REPORT OR ANY INFORMATION, APPARATUS, METHOD, PROCESS, OR SIMILAR ITEM DISCLOSED IN THIS REPORT.

ORGANIZATION(S) THAT PREPARED THIS REPORT

Ishikawajima-Harima Heavy Industries Company, Limited, 3-1-15 Toyosu, Koto-ku, Tokyo 135, Japan

ORDERING INFORMATION

Cost: $15,000

Requests for copies of this report should be directed to the EPRI Distribution Center, 207 Coggins Drive, P.O. Box 23205, Pleasant Hill, CA 94523, 510/934-4212.

Electric Power Research Institute and EPRI are registered service marks of Electric Power Research Institute, Inc.

Copyright © 1998 Electric Power Research Institute, Inc. All rights reserved.

REPORT SUMMARY

A nondestructive method has been developed to characterize the microstructural changes induced in nuclear power plant materials resulting from the accumulation of fatigue damage prior to macro-crack initiation. These microstructural changes can be correlated with the amount of damage even in the early stages of fatigue and provide insight into the prediction of remaining component life.

Background

The factors that lead to fatigue cracks in structures and components are well known. However, knowledge of when fatigue cracks actually begin and their rate of propagation within a structure is not well understood. The ability to detect, via actual measurement, the onset of significant fatigue followed by crack initiation prior to failure should significantly improve component life prediction capabilities. If a correlation between pre-fatigue damage and associated microstructural changes could be obtained, the accuracy of present life assessment methodologies could be enhanced, corrective measures could be made more efficient, and a technique to ensure the reliability of refurbished structures and components should be feasible. A successful fatigue measuring technique could potentially be used to assess the structural integrity of a broad range of structures and components.

Objectives

- To develop a technique to measure microstructural changes in materials due to accumulated fatigue damage.
- To quantitatively correlate changes in microstructure to fatigue damage level.
- To assess the potential for application of this technique to improved life assessment capabilities.

Approach

An effective method for measuring the fatigue damage accumulation state in a structural material was identified and applied. The method, selected area diffraction (SAD), is a microstructural examination technique that is used for identifying small cell-to-cell angular misorientations in the crystal lattice of a material. It was observed that this misorientation can be correlated quantitatively to fatigue damage level. Fatigue damage was induced in samples taken from an SA508 steel plate by various loading histories in order to examine the influence of prior cyclic loading below and above the fatigue limit. Angular misorientation measurements were taken on these samples utilizing the SAD technique. The SAD measurements were then correlated with the total fatigue damage in the samples.

Results

The results from this work indicate that SAD measurements can be correlated with accumulated fatigue damage in the materials tested. A critical misorientation threshold value was suggested by the data, above which samples consistently exhibited macro-crack initiation. The extent of pre-cycling, even for as few as 10 cycles or 100 cycles, significantly affected the material's overall fatigue life. These changes were quantitatively measured with the SAD technique.

EPRI Perspective

This project is a multiyear effort with leveraged funding through Ishikawajima-Harima Heavy Industries Co., Ltd. (IHI) in Japan. Phase I activities were completed in 1997 and included additional sample testing to determine the impact of pre-cycling and strain hardening/softening on overall fatigue life and the correlation of results with data obtained from SAD measurements. Phase II (1998) will involve additional sample testing in reactor water environments to help resolve industry license renewal issues regarding the impact of environment on component fatigue life. In addition, Phase II will involve testing at different strain range levels to refine the correlations previously observed in Phase I between angular misorientation and accumulated fatigue damage. Phase I results are documented in this report. Phase II activities will be documented in an EPRI report to be published in April 1999.

TR-110250

Interest Categories

Piping, reactor vessel, and internals

Plant life cycle management

Keywords

Fatigue

Component integrity

Selected area diffraction

ABSTRACT

An effective method for measuring the fatigue damage accumulation state in a structural material was identified and applied. The method, selected area diffraction (SAD), is a microstructural examination technique that is used for identifying small cell-to-cell angular misorientations in the crystal lattice of a material. It was observed that this misorientation can be correlated quantitatively to fatigue damage level. Fatigue damage was induced in samples taken from an SA508 steel plate by various loading histories in order to examine the influence of prior cyclic loading below and above the fatigue limit. Angular misorientation measurements were taken on these samples utilizing the SAD technique. The SAD measurements were then correlated with the total fatigue damage in the samples.

Fatigue test bars fabricated from SA508 were cyclically deformed under different loading regimes to investigate the influence of loading sequences on the fatigue life, with special consideration given to the early stages of cycling. Specimens were subjected to high-to-low and low-to-high amplitude cyclic strain, including both below (total strain range of 0.40%) and above (total strain range of 0.62%) the fatigue limit. High-to-low loadings initially included 10 cycles and 100 cycles of high strain range loadings. These small numbers of cycles were less than 1% of the total lifetime when the specimens were subjected to the constant amplitude fatigue test. Specimens were then cut perpendicular to the stress axis within the gage section at a minimum distance of 5 mm from any observable cracks. Transmission electron microscopy (TEM) was utilized to obtain microstructural characteristics of the samples, and cell-to-cell angular misorientation differences were measured by the SAD method. Surface cracking was also observed by the surface replication technique.

The electron backscattering diffraction patterns (EBSP) technique was applied to specimens previously measured using the SAD technique in order to compare results and evaluate application of the two techniques. Crystallographic orientation data were analyzed to determine the feasibility of this technique for measuring the state of fatigue damage accumulation. The results were compared with the SAD measurements previously performed on the same material to determine the preferred method for quantitatively measuring fatigue damage. EBSP images were obtained from the SA508 specimens, even though the material had well-developed cell structures and a high dislocation density. The orientation imagings drawn from the EBSP data were similar to observed TEM images.

ACKNOWLEDGMENTS

This report was prepared by C. Fukuoka and Y. G. Nakagawa of Ishikawajima-Harima Heavy Industries Company, Limited, in Tokyo, Japan. TEM work was performed in the electron microscopy facility of the Tokyo Research Institute at IHI.

CONTENTS

FIGURES

TABLE

1

INTRODUCTION

This report documents the Phase I efforts under a two-phase joint project with Ishhikawajima-Harima Heavy Industries Co., Ltd., (IHI) in Japan. The principal objective of this project is to investigate techniques for measuring the early stages of fatigue in reactor component materials. The objectives of Phase I (1997) were to:

1. clarify the loading history effect (impact of pre-cycling and strain hardening/softening) on the fatigue life of SA508 reactor pressure vessel forging material in terms of microstructural changes
2. determine a correlation between the microstructural phenomena and the lifetime change with regard to loading history via the selected area diffraction (SAD) technique
3. investigate the feasibility of using the electron backscattering diffraction patterns (EBSP) technique for sample measurement in order to take advantage of the easier sample preparation and sample measurement associated with this technique

The results of these activities are discussed in this report.

Section 2 provides background information regarding the microstructural techniques utilized in this project and previous EPRI research in this area that led to this joint effort with IHI. Section 3 discusses the structure of the joint EPRI/IHI program. Section 4 summarizes the experimental procedures utilized in this study. Section 5 discusses the SAD results, and Section 6 presents the EBSP results. Conclusions are provided in Section 7.

Phase II (1998) will involve additional sample testing in reactor water environments to characterize the impact of environment on component fatigue life. In addition, Phase II will involve testing at different strain range levels to refine the correlations previously observed in Phase I between angular misorientation and accumulated fatigue damage.

2

BACKGROUND

The factors that lead to fatigue cracks in structures and components are well known. However, knowledge of when fatigue cracks actually begin and their rate of propagation within a structure is not well understood. The ability to detect, via actual measurement, the onset of significant fatigue damage that ultimately leads to macro-crack initiation should significantly enhance component life assessment capabilities and repair/replacement strategies. A successful fatigue measuring technique could be used to assess the structural integrity of a broad range of structures and components. The ability to measure—and, more importantly, predict accumulated fatigue damage—should provide a more economical and reliable approach to component life assessment.

The experiments described in this report were inspired by the observation in earlier work that the fatigue life of pressure vessel steels, such as SA508, depends on the fatigue testing sequence and is strongly related to the microstructural changes during fatigue [1,2,3,4,5]. Specimens that have been pre-cycled for 10^6 cycles below the fatigue limit, when subsequent cycling is carried out at total strain ranges above the fatigue limit, showed an increase in fatigue life of about 50% from the original lifetime. In contrast, specimens that have been pre-cycled above the fatigue limit subsequently failed even when cycled below the fatigue limit. As the latter type of loading is consistent with inservice components, knowledge of the lifetime change due to loading history is important.

It has been established that the cumulative fatigue ratio, $\Sigma(n / N)$—where n is the number of cycles and N is the total number of cycles—is usually greater than unity for steels when low stress is applied first, while it is usually less than unity when high stress is applied first [6,7,8,9]. Specifically, the fatigue resistance of some metals can be improved by stressing below the fatigue limit followed by a process of gradually increasing the amplitude of the alternating stress in small increments, a procedure called coaxing. This phenomenon has been explained in terms of strain aging [10].

Others have also reported that the fatigue life was increased by pre-cycling at a low stress followed by a gradual increase in stress even after crack initiation during pre-cycling [11]. This effect was explained by small crack growth and its relation to the plastic zone of the previous loading. The fatigue limit increased only when the stress level increment was sufficiently small so that the crack growth occurred within the deformation zones in the vicinity of the crack tip after the stress increase, resulting in crack retardation.

In contrast, the transition between the two strain ranges in previous EPRI research was significantly larger than what could be explained by the preceding hypothesis. It was also found that changes observed in the microstructure correlated well with the change in fatigue lifetime and that this microstructural observation could be used to evaluate the remaining lifetime of components. The effect of variable amplitude loading on fatigue lifetime has been previously investigated, but most of these focused on the crack propagation stage [12]. An objective of this work was to clarify the loading history effect on the fatigue lifetime of SA508 in terms of microstructural changes and to determine a correlation between the microstructural phenomena and the lifetime change with regard to loading history. This study specifically focused on fatigue life when the cycling included loadings below the fatigue limit.

Under previous EPRI research, an effective method for measuring the fatigue damage accumulation state in a pressure vessel material was identified and applied. The method, SAD, is a microstructural examination technique used for identifying small cell-to-cell angular misorientations in the crystal lattice of a material. It was observed that this misorientation, which is a prerequisite for crack initiation and propagation, can be correlated quantitatively to fatigue damage level. The SAD technique was demonstrated on samples taken from pressurized water reactor (PWR) feedwater nozzles. It was effective in measuring the microstructural damage state of the material exposed to actual service conditions in a power plant.

The SAD technique was also utilized to evaluate the damage induced below and above the fatigue limit. Fatigue damage was induced in samples taken from an SA508 steel plate by various loading histories in order to examine the influence of prior cyclic loading below the fatigue limit. It was found that fatigue test bars had a longer lifetime after pre-cycling below the fatigue limit, while pre-cycling above the fatigue limit caused other specimens to fail even when subsequently cycled below the fatigue limit.

It has been demonstrated that the SAD technique can quantify the microstructural damage state during fatigue accumulation in SA508 steel [1,2,3,4,5]. However, the SAD method requires lengthy sample preparation and extensive transmission electron microscopy (TEM) work in order to obtain the measurements necessary for a statistically adequate determination of angular misorientation. An additional objective of this study was to investigate alternate techniques that would provide information similar to that obtained via the SAD technique but in a simplified manner.

Recently, electron backscattering diffraction patterns (EBSP) have been developed as an automatic computerized processing technique to obtain crystallographic information [13,14]. This technique, combined with scanning electron microscopy (SEM), provides for the collection of detailed lattice orientation information from a small localized region. The electron backscattered Kikuchi lines, an artifact of inelastic scattering during electron beam diffraction, are used in EBSP [15].

Theoretically, this technique is capable of obtaining the same information as the SAD technique, which utilizes elastic electron scattering. As the EBSP is performed in the SEM, the sample preparation procedure becomes simplified and an observable sample area can be significantly enlarged. Statistical information should be easily obtained by EBSP. As part of this project, the EBSP technique was used to measure the angular misorientation of SA508B samples as a function of accumulated fatigue damage and the results compared to those obtained through the SAD technique.

3

PROGRAM STRUCTURE

Task 1 of the joint EPRI/IHI Phase I effort focused on further investigating the effect of loading history on the fatigue life of a reactor pressure vessel forging material, type SA508. The fatigue life of pressure vessel steels depends on the fatigue testing sequence and is strongly related to the microstructural changes during fatigue [1,2,3,4,5]. Specimens that have been pre-cycled below the fatigue limit when subsequent cycling was carried out at total strains above the fatigue limit showed an increase in fatigue life of about 50% from the original life. In contrast, specimens that were pre-cycled above the fatigue limit subsequently failed even if cycled below the fatigue limit. As the latter loading is consistent with inservice components, knowledge of the change in fatigue life due to loading histories is important. Under Task 1, various combinations of fatigue testing were performed at two strain range values: one at a level below the fatigue endurance limit for the material that was not expected to result in fatigue failure, and the second at a level that was expected to produce fatigue failure after a nominal number of cycles. The various combinations of these different strain range levels, their impact on overall fatigue life, and correlation of these results with microstructural measurements performed using the SAD technique were investigated.

As previously discussed, the SAD technique requires extensive TEM analysis to adequately characterize angular misorientation between cell substructures. Task 2 of the joint EPRI/IHI Phase I effort focused on investigating the feasibility of an alternate technique that would provide information similar to that obtained via SAD but would allow for easier sample preparation. The SAD technique has been demonstrated as a useful tool to quantify the microstructural damage during fatigue in quench and tempered steels. A concern regarding the commercial application of SAD is that the technique requires time-consuming sample preparation and extensive TEM observations. The EBSP technique, combined with SEM, might provide the ability to obtain detailed lattice orientation information in small localized regions. Theoretically, this technique is capable of obtaining the same information as the SAD technique, which utilizes elastic electron scattering. As the EBSP method is performed in the SEM, the sample preparation procedure becomes simplified and the observable area for fatigue examination can be significantly enlarged. The EBSP technique was investigated in this task and its feasibility for application to fatigue measurement evaluated.

Task 1: Fundamental Fatigue Mechanisms

The objective of Task 1 was to further investigate the effect of loading history on the fatigue life of SA508 plate forging material. Fatigue loadings, specifically including those below the fatigue limit, were investigated. Fatigue-induced cracks were observed using a surface replication technique. The SAD technique was used to correlate the microstructural phenomena associated with accumulated fatigue damage and the lifetime change due to the loading history.

Task 2: Feasibility Study—Electron Backscattering Diffraction Patterns (EBSP) Method

The objective of Task 2 was to investigate the feasibility of the EBSP method for estimating the remaining fatigue lifetime of the SA508 samples. Samples subject to fatigue accumulation were measured by the EBSP methods and the results compared with those obtained through the SAD technique.

4

EXPERIMENTAL PROCEDURE

SAD Measurements

Fatigue test bars were machined from an SA508 class 2 low-alloy steel forging material. The chemical composition, heat treatment history, and major mechanical properties of this material are summarized in Table 1. Figure 1 provides the fatigue test bar dimensions. For the SAD measurements, fatigue damage was induced in the test bars by both strain- and stress-controlled cycling at two different strain ranges, 0.40% and 0.62%, at 300°C. Sample failure was taken to be the point beyond which the applied stress fell 10% under the same strain conditions.

Table 1
Chemical Composition, Mechanical Properties, and Heat Treatments of SA508 Plate

	C	Si	Mn	P	S	Ni	Cr	Mo
Weight %	0.19	0.26	0.69	0.004	0.001	0.87	0.37	0.65

YS = 504 MPa, TS = 645 MPa, El. = 28.3%, FL = 360MPa

Heat treatment		Temperature (°C)	Time (h)	Cooling
Refining	quenching	855	8.5	WQ
	tempering	655	4.5	AC
Stress relieving		630	45	FC

Note: YS = 0.20% offset yeild strength; TS = tensile strength; El. = % elongation to failure;
FL = Fatigue Limit for this heat, AC = air-cooled; FC = furnace-cooled; and WQ = water-quenched.

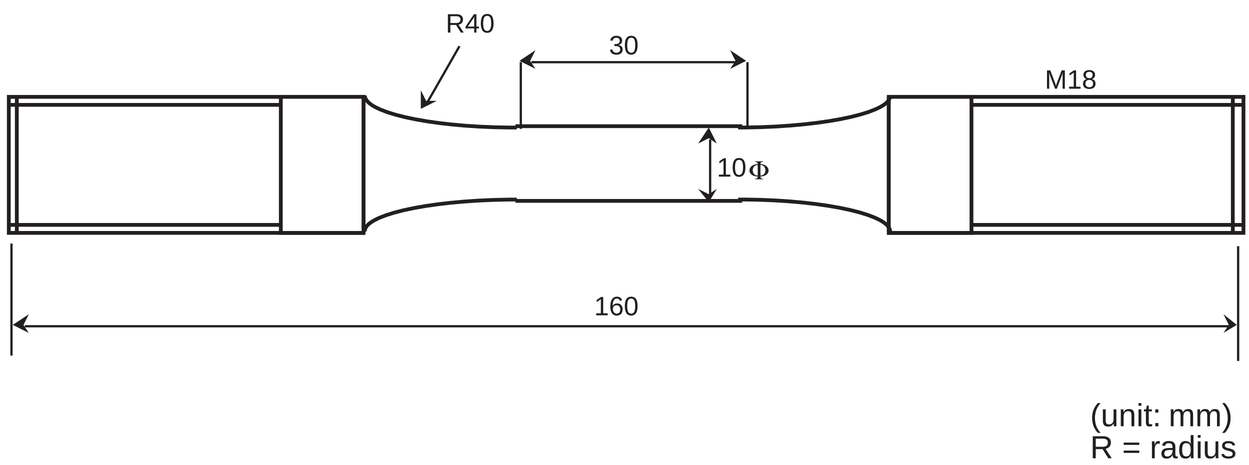

Figure 1
Fatigue Test Bar Dimensions

The testing sequences consisted of three types of loading history, as shown schematically in Figure 2. In the first type (I), test bars were subjected to a total strain range of 0.62%, an amplitude above the fatigue limit, until failure by strain-controlled tests (at 1.6 Hertz / Hz). The second type (II) involved pre-cycling to $1x10^6$ cycles at a total strain range of 0.40%, an amplitude below the fatigue limit, followed by cycling at a total strain range of 0.62% until failure. The third test series (III) involved pre-cycling above the fatigue limit at a total strain range of 0.62% (at 1.6 Hz) for 10 cycles or 100 cycles followed by $1x10^6$ cycles at 0.40% total strain range (below the fatigue limit) at 4.0 Hz and then cycling again at 0.62% total strain range (above the fatigue limit) at 1.6 Hz until failure. The stress ranges (0.40% and 0.62%) for these tests had been determined previously so that the strain range chosen for subsequent testing below the fatigue limit should contain plastic strain [1].

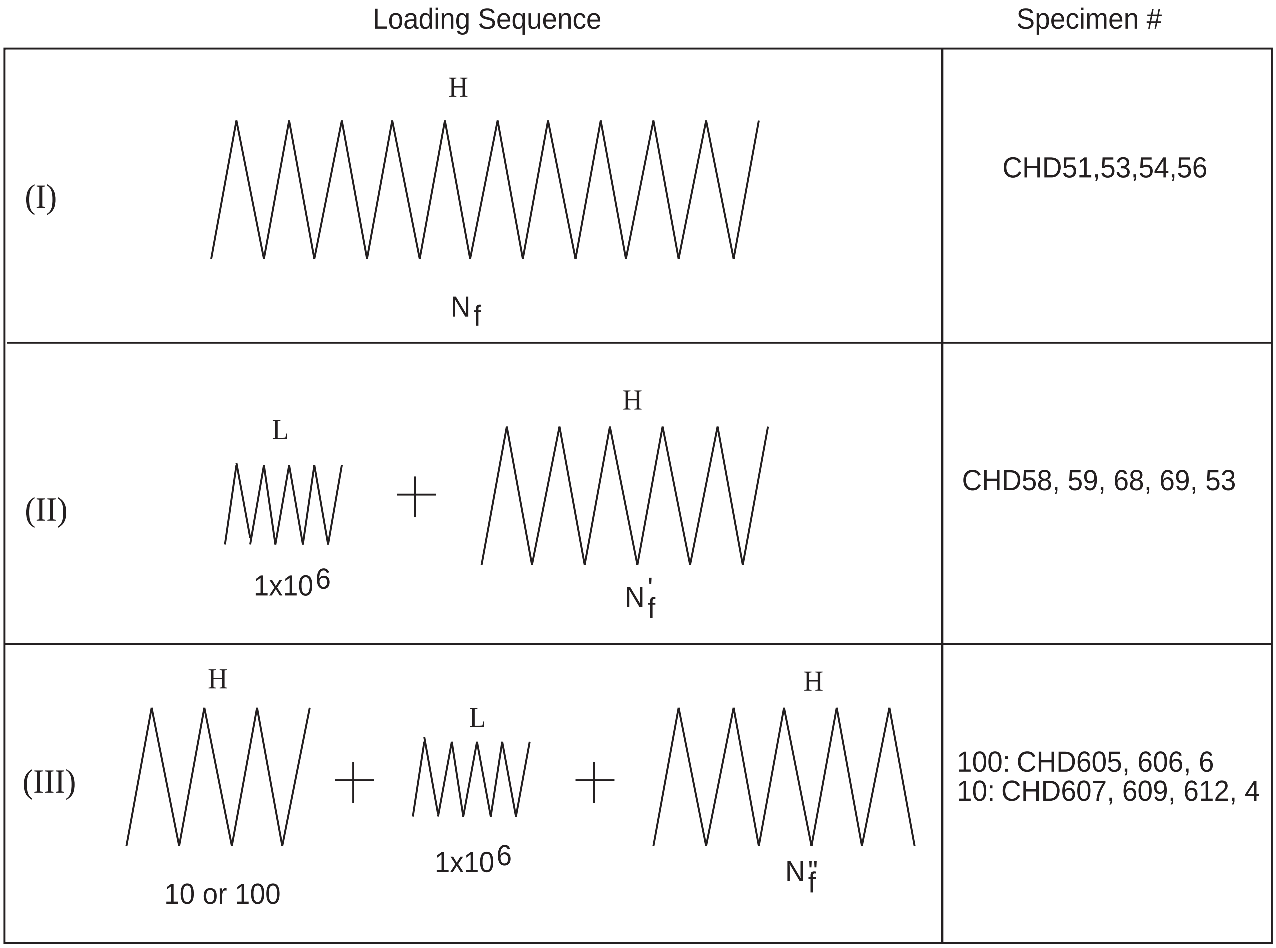

Note: H: strain-controlled test at a total strain range of 0.62%
L: strain-controlled test at a total strain range of 0.40% for 30,000 cycles (until stress saturation) followed by stress-controlled test at the stress equal to the saturation point

Figure 2
Schematic Illustration of Testing Sequence for Constant Amplitude and Multiple Amplitude Fatigue

Cyclic microstructural changes below the fatigue limit were induced by a combination of both strain-controlled testing and stress-controlled testing [1]. This combination involved conducting strain-controlled tests until stress saturation occurred, followed by stress-controlled tests at a stress value equal to the stress at the saturation point. This procedure is similar to strain-controlled testing, but it allows fatigue tests below the fatigue limit (consisting of as many as $1x10^6$ cycles) to be completed much faster than strain-controlled testing alone.

Those samples whose fatigue tests were interrupted for microstructural examination were first visually inspected for cracking; for some specimens, surface replicas were taken from the gage section and examined with an optical microscope (100, 200, and 500 times magnification).

All test bars were cut perpendicular to the stress axis within the gage section at a minimum location of 5 millimeters (mm) from any visible cracks. Small disks (3 mm diameter x 0.1 mm thickness) were fabricated and electropolished to prepare TEM and SAD samples having an approximate thickness of 0.2 nanometers (nm) to 100 nm. The TEM machine used in this experiment was a Hitachi 700H operating at 200 kilovolts (kV).

Microstructural damage was evaluated by the SAD method and correlated to the fatigue test regimen. Heat treatment was also performed at 300°C for approximately 2.5 hours on a single sample in order to determine if the test temperature itself contributed to the cell-to-cell angular misorientation decrease observed during low cycle fatigue after cycling below the fatigue limit. Fatigue lifetime changes due to the different types of testing sequences were correlated to the microstructural observations by the SAD method and surface observations.

EBSP Measurements

A majority of the samples analyzed via the EBSP technique were previously analyzed using SAD in order to directly compare capabilities of the two techniques. Fatigue test bars were machined from an SA508 class 2 low-alloy steel forging material. The chemical composition, heat treatment history, and major mechanical properties of this material were summarized in Table 1. Figure 1 provides the fatigue test bar dimensions. For the EBSP measurements, fatigue damage was induced in the test bars by strain-controlled cycling at a total strain range of 0.62% at 300°C. Sample failure was taken to be the point beyond which the applied stress fell 10% under the same strain conditions. At this point, the fatigue tests were terminated. The fatigue test conditions utilized for EBSP measurements are summarized in Table 2.

Table 2
Fatigue Test Conditions for EBSP Measurement

Specimen #	Total Strain Range (%)	Temperature (˚C)	Number of Cycles	N/N_f (%)
As-Received	-	-	-	0
CHD611	0.62	300	10	0.083
CHD610	0.62	300	100	0.83
CHD9	0.62	300	1,200	10
CHD10	0.62	300	3,000	25
CHD65	0.62	300	6,000	50
CHD53	0.62	300	12,360	100
CHD54	0.62	300	11,500	100

Test bars were cut perpendicular to the stress axis within the gage section, at a minimum location of 5 mm from any visible cracks. Wafers approximately 1 mm–2 mm thick were removed from each specimen, subsequently polished and electropolished to prepare EBSP samples.

The SEM utilized in this study was a Phillips XL-30 with a LaB_6 gun operating at 25 kV. The same system was also used with a field emission gun. For crystallographic orientation analysis, the SEM was equipped with a TSL orientation imaging microscopy (OIM) EBSP system.

5

MICROSTRUCTURAL INVESTIGATION FOR LOADING SEQUENCE EFFECTS ON FATIGUE LIFE

SAD Microstructural Examination

Microstructural examination in this study utilized the SAD technique. The method is schematically illustrated in Figure 3. This method utilizes TEM to measure the average cell-to-cell misorientation in grains oriented around the <111> zone axis. An example of the statistical analysis performed on data obtained from the SAD technique is shown in Figures 4a–c. The normal distribution of the maximum angular deviation, q, is illustrated for an as-received SA508 sample and for samples previously fatigued at a total strain range of 0.78% to N / N_f = 50, 100% (N_f = 2,100). The fraction of life, N / N_f, expresses the state of fatigue damage, where N is the number of the cycles applied to the sample and N_f is the number of cycles to failure. The mean value of q, equivalent to probability in each plot, is considered to represent an average angular deviation of the cells from the reference direction, <111>.

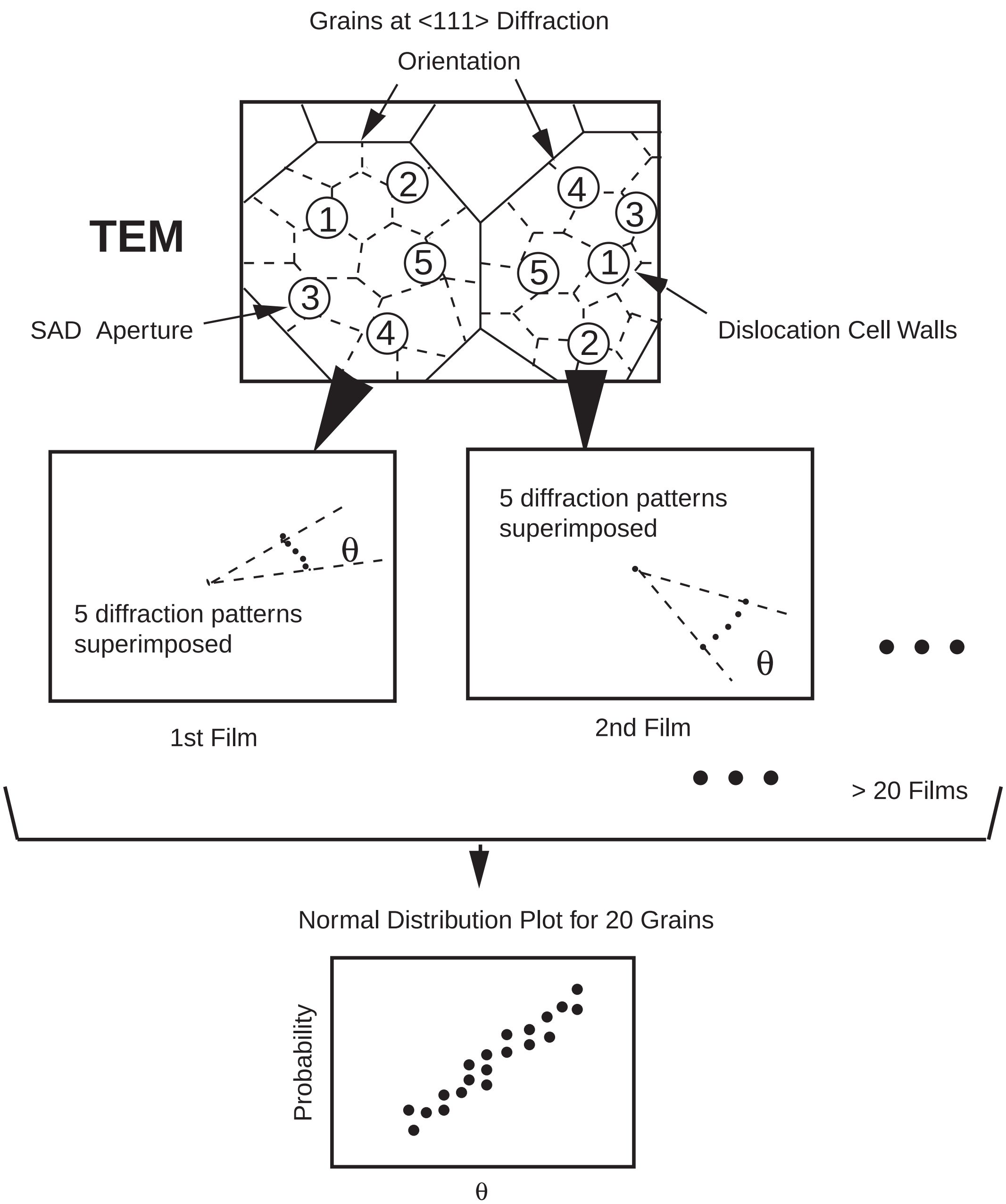

Figure 3
Schematic Illustration of the SAD Procedure

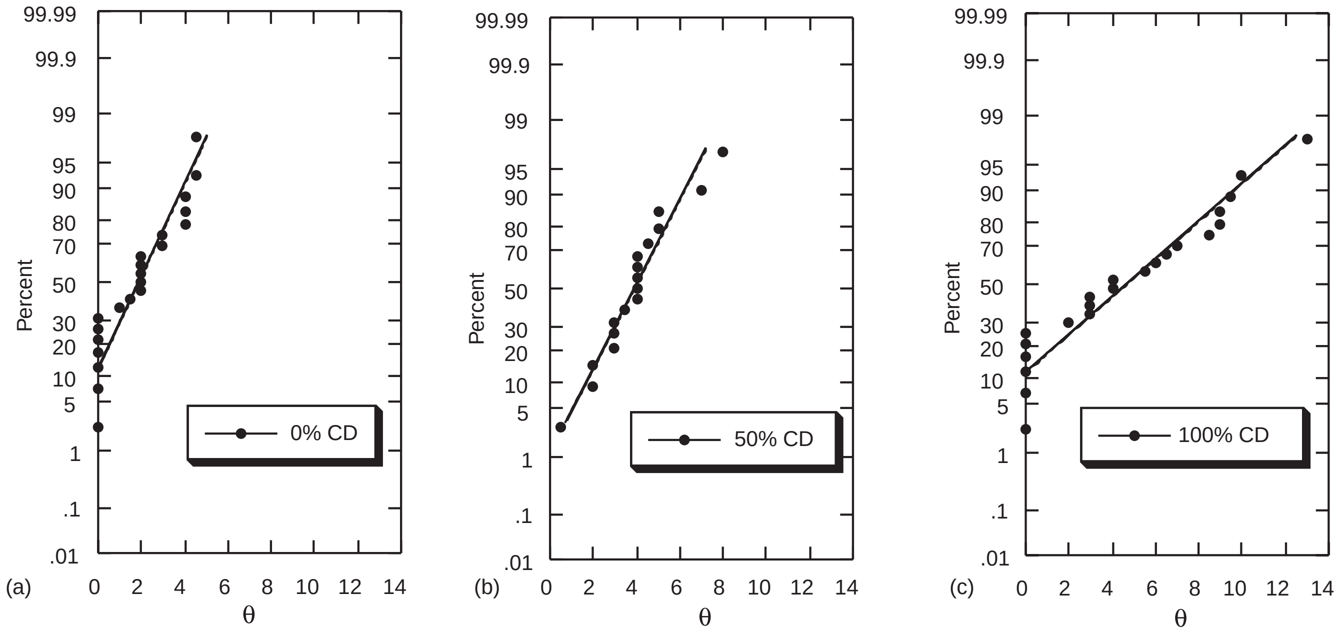

Figure 4
Normal Distribution of the Cell Orientation, θ, of Fatigue Life for Samples Cycled at a Total Strain Range of 0.78%: (a) for 0% (b) for 50%, and (c) for 100%
(Note: CD = cumulative damage.)

Results and Discussion

The fatigue test conditions utilized in this study and the corresponding SAD measurement results are summarized in Table 3 and graphically presented in Figure 5. As shown in Figure 5, the loading history has a significant effect on fatigue life. In this figure, the horizontal axis represents the number of cycles applied to the specimen at a total strain range, $\Delta\varepsilon_t$, of 0.40%, and the vertical axis represents the number of cycles applied at $\Delta\varepsilon_t$ = 0.62%. A total strain range of 0.40% is considered to be below the fatigue limit for this material. If the cycling below the fatigue limit does not affect the total lifetime of the sample as mathematically described in Miner's rule, cycling at 0.40% total strain range should have no effect on the lifetime (the dashed line in Figure 5). The vertical location of the dashed line was determined by the average number of cycles to failure for normal fatigue testing at a total strain rage of 0.62%. The solid line is a linear extrapolation of the S-N curve above the fatigue limit generally termed Modified Miner's rule. As the 0.40% total strain range is very close to the fatigue limit, the lifetime of a specimen cycled at a total strain range of 0.40% is assumed as 10^6 cycles.

Table 3
Fatigue Test Conditions and Results

	Specimen#	Total Strain[1] (%)	Stress (*)[2] (MPa)	N_f	Notes	SAD (deg)
	As-Received					1.9
(I)	CHD51	0.62	417	12,175	3	4.4
	CHD53	0.62	415	12,360	3	4.0
	CHD54	0.62	412	11,500	3	
	CHD55	0.62	413	10,311	3	
	CHD56	0.62	415	13,630	3	
	CHD65	0.62	408	6,000	interrupted, cracks, rep	3.1
	CHD610	0.62	434	100	interrupted, rep	2.5
	CHD611	0.62	427	10	interrupted, cracks, rep	2.2
below the fatigue limit						
	CHD64	0.40+ 354MPa(eq)	354	30,000 9.7E5	interrupted, cracks, rep	3.3
	CHD7	0.40	353	30,000	interrupted, cracks, rep	2.7
heat treated at 300˚C for 2.5 hours after fatiguing						
	CHD64H	0.40+ 354MPa(eq)	354	30,000 9.7E5	interrupted+heat treated	3.5
low to high						
(II)	CHD58	0.40+ 354MPa(eq) + 0.62	354 410	30,000 9.7E5 18,320	4	4.6
	CHD59	0.40+ 356MPa(eq) + 0.62	356 410	30,000 9.7E5 19,140	4	
	CHD68	0.40+ 357MPa(eq) + 0.62	357 413	30,000 9.7E5 3,000	interrupted	3.1
	CHD69	0.40+ 354MPa(eq) + 0.62	354 413	30,000 9.7E5 6,000	interrupted	2.5
	CHD52	0.40+ 356MPa(eq) + 0.62	356 403	30,000 9.7E5 10,000	interrupted	2.7
high100 to low (to high)						
(III)	CHD605	0.62+ 0.40+ 356MPa(eq)+ 0.62	422 356 424	100 30,000 9.7E5 9,225	4	4.0
	CHD606	0.62+ 0.40+ 358MPa(eq)	433 358	100 30,000 7.07E5	3 (failed during cycling below the fatiuge limit)	
	CHD6	0.62+ 0.40+	417 342	100 30,000	interrupted, cracks, rep	3.9

Table 3 (continued)
Fatigue Test Conditions and Results

	Specimen#	Total Strain[1] (%)	Stress (*)[2] (MPa)	N_f	Notes	SAD (deg)
high10 to low to high						
(III)	CHD607	0.62+ 0.40+ 360MPa(eq)+ 0.62	426 360 421	10 30,000 9.7E5 19,363	3	4.3
	CHD609	0.62+ 0.40+ 360MPa(eq)+ 0.62	421 360 394	10 30,000 9.7E5 18,154	3	4.3
	CHD612	0.62+ 0.40+ 358MPa(eq)	426 358	10 30,000 9.7E5	interrupted, cracks, rep	3.7
	CHD4	0.62+ 0.40+	413 354	10 30,000	interrupted, cracks, rep	3.0

Notes:

[1] Total Strain

- 0.62% @ N_f; Avg. N_f = 11,995 (CHD51, 53-56)
- 0.40% @ 30,000 + 336 MPa @9.7 E5 + 0.62% @ N_f; Avg. N_f = 18,730 (CHD58-59)
- 0.62% @ 100 + 0.40% @ 30,000 + 356 MPa @ 9.7E5 + 0.62% @ N_f; N_f = 9,225 (CHD605)
- 0.62% @ 100 + 0.40% @ 30,000 + 358 MPa @ 707,267 (failed - CHD606)
- 0.62% @ 10 + 0.40% @ 30,000 + 360 MPa @ 9.7E5 + 0.62% @ N_f; Avg. N_f = 18,759 (CHD607, 609)

[2] Stress amplitude ($\Delta\sigma_t/2$) at $N_f/2$ or when test terminated.

[3] Sample failure within gage section.

[4] Sample failure within 25% of gage length center.

rep = Surface observation by replication technique was performed.

eq = Stress-controlled test to obtain strain level similar to that of prior strain-controlled test.

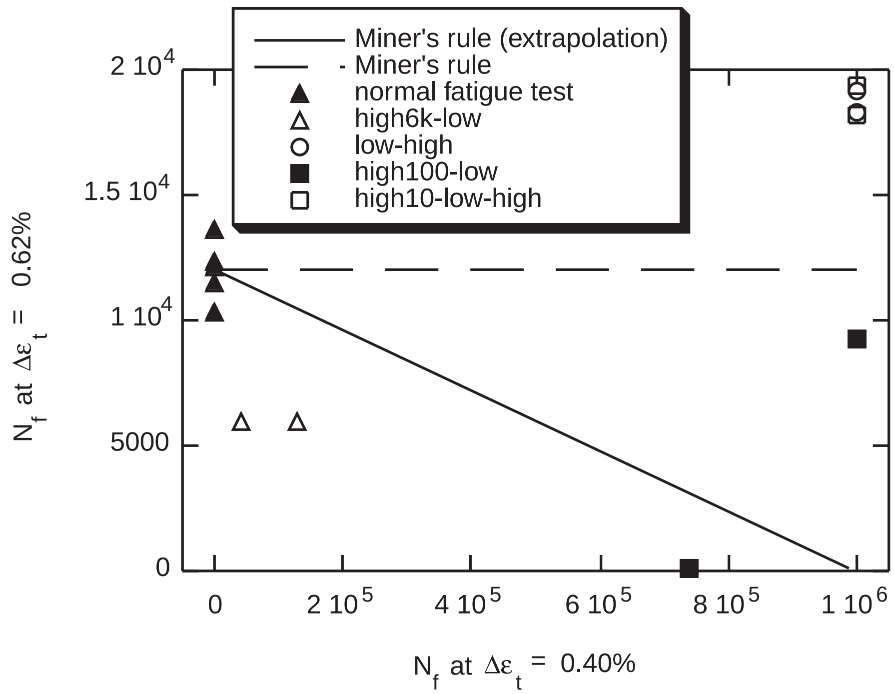

Figure 5
Relationship between Loading History and Fatigue Life

The solid triangle markers represent normal fatigue test sequence results. For this case, testing was performed at 0.62% with failure occurring after an average of 12,000 cycles. The remaining markers represent different loading histories. Open triangles represent testing for 6,000 cycles at 0.62% followed by loading at 0.40% until failure. Open circles represent testing for 10^6 cycles at 0.40% followed by 0.62% strain range cycling until failure. Open and closed square markers represent initial testing to 10 cycles and 100 cycles, respectively, at a total strain range of 0.62% followed by cycling at a total strain range of 0.40% until failure or 1 x 10^6 cycles, whichever occurred first. If failure did not occur after 10^6 cycles, the sample was cycled again at a total strain range of 0.62% to failure (open square markers).

For the low-high loading sequence (open circles in Figure 5) and high10-low-high loading sequence (open squares in Figure 5), the fatigue lifetime is significantly extended when compared to normal fatigue loading performed without pre-cycling. However, the high100-low loading sequence (closed squares in Figure 5) reduced the fatigue lifetime when compared to fatigue testing at 0.40% without pre-cycling. Note that fatigue cycling for less than one percent of the normal testing lifetime at the beginning of fatigue testing sequence significantly effected the remaining fatigue life.

The cyclic strain softening (and hardening) behavior of SA508 is shown in Figures 6a and 6b. The stress amplitude remains almost constant for a strain range below the fatigue limit (0.40% in Figure 6a), while the material cycled at the higher strain range level (0.62%) work hardens for approximately 100 cycles, after which work softening occurs (Figure 6b). The initial number of cycles performed at higher amplitude was interrupted at 10 cycles and 100 cycles in order to investigate the importance of the cyclic hardening effect on the fatigue lifetime. However, no strong influence on lifetime from the cyclic hardening effect was observed through these experiments as will be discussed later.

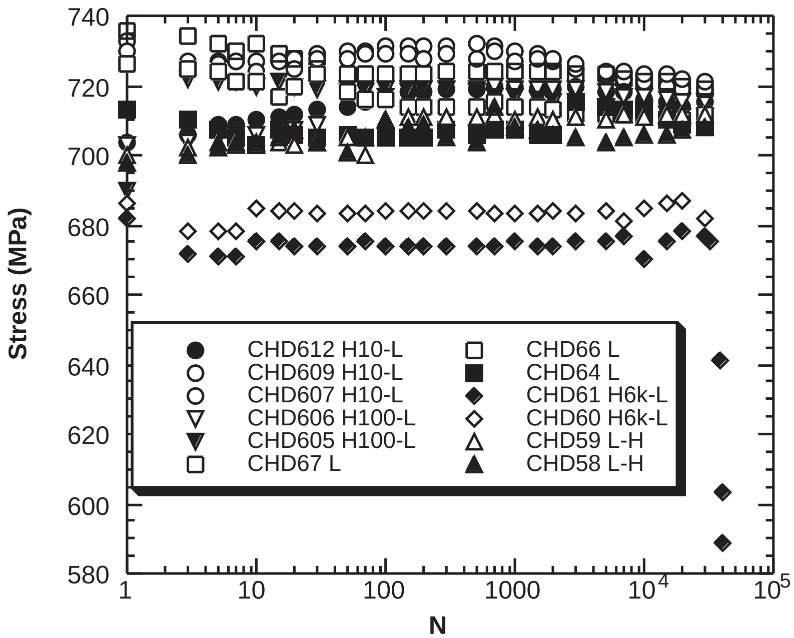

(a) 0.40% total strain range

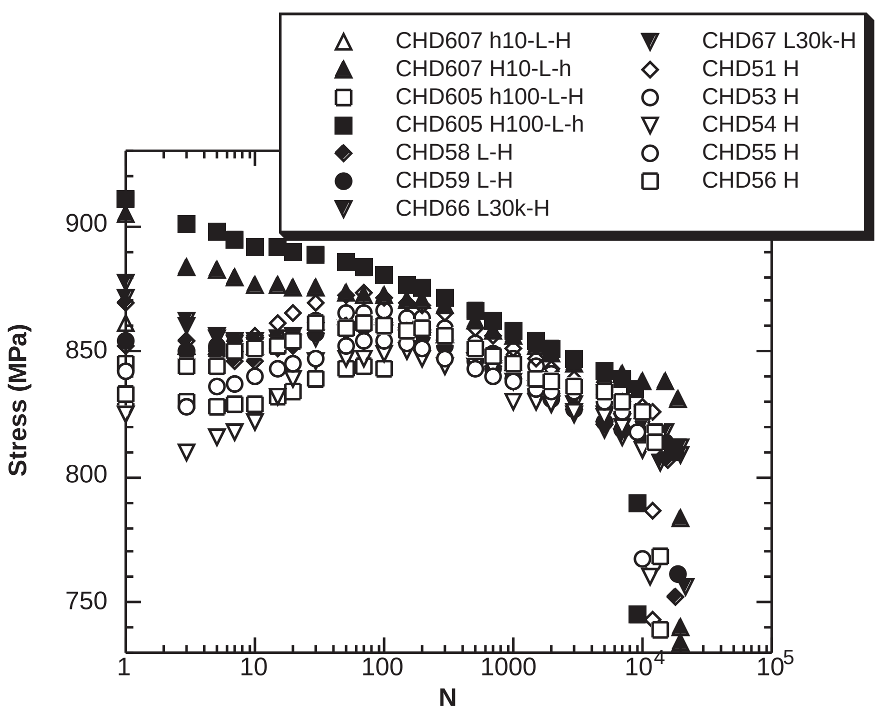

(b) 0.62% total strain range

Figure 6
Cycle Behavior of SA508 (a) at 0.40% Total Strain Range and (b) at 0.62% Total Strain Range

Several specimens showed slight work softening, while others showed slight hardening; however, the saturation stresses were similar in either case, as shown in Figure 6a when the specimens were subjected to stresses below the fatigue limit. Stresses are much lower (approximately 30 megapascals (MPa) lower) when pre-cycling (for 6,000 cycles at 0.62% strain range) was conducted (see specimens CHD61 and CHD60) but are equivalent to those samples without pre-cycling when the pre-cycling was conducted for 10 cycles or 100 cycles. This may be due to the cyclic softening during fatigue at the higher strain ranges. When this material is exposed to a relatively higher strain range of 0.62%, it begins to work soften after approximately 100 cycles, as shown in Figure 6b. However, the lifetime of the specimen pre-cycled for 100 cycles was shorter than the original lifetime even though pre-cycling for 10 cycles or 100 cycles did not affect the cyclic stresses, as shown in Figure 6a.

In Figure 6b, solid triangle and solid square markers represent specimens pre-cycled for 10 cycles and 100 cycles, respectively, at 0.62% total strain range prior to pre-cycling below the fatigue limit (total strain range of 0.40%) followed by cycling to failure at 0.62% total strain range. The first two sequences for each sample lead to an overall strain softening throughout fatigue cycling at the higher strain amplitude, but the lifetime was quite different for these two cases. Fatigue life was strongly related to the loading regimen, but no significant correlation was found between cyclic softening behavior and lifetime of the samples.

In order to observe microstructural changes in the samples, several fatigue tests were stopped before failure. (Many of these were not expected to fail even if cycling was continued, due to being strained below the fatigue limit.) The SAD and the TEM methods are considered to be nondisruptive investigation techniques, which require that only a small amount of material be sampled in relation to the size of the component. However, these techniques are effectively destructive for the small laboratory specimens.

Replica observation was performed for samples whose fatigue test was interrupted at (1) 10 cycles, 100 cycles, and, 6,000 cycles with a total strain range of 0.62%, (2) 30,000, and 10^6 cycles with a total strain range of 0.40%, and (3) various other combinations, as shown in Table 3.

The replication method proved very effective in identifying small cracks, but it was a time-consuming procedure. Ideally, the replication method should be applied to specimens during the fatigue test. However, there might be artifacts induced by interrupting the fatigue tests because the tests are performed within an inductance heating coil at 300°C and by dismantling and reassembling the test apparatus. Therefore, partially fatigued samples were examined using the replication method and the results assumed to apply to similar samples undergoing the full fatigue test.

Small cracks found by the replication method are shown in Figures 7a–c. Cracks were observed even for specimens tested below the fatigue limit or for specimens cycled only to 10 cycles or 100 cycles (less than 1% of the total lifetime). It has been reported that crack initiation can occur immediately, and that cracks subsequently arrest when they grow beyond grain boundaries [16,17]. As shown in Figures 7a–c, however, the size of cracks found in the samples are larger than the average grain size (15 micrometers (mm) to 20 mm) of the specimens. It should also be noted that the size of the cracks found at the specimen surfaces are similar in size (50 mm); in other words, crack initiation occurs at a very early stage of the fatigue test, but in most cases, crack growth does not occur until near the end of the lifetime. Under certain fatigue conditions, such as the low-high loading sequence or the high10-low-high loading sequence, crack growth is arrested.

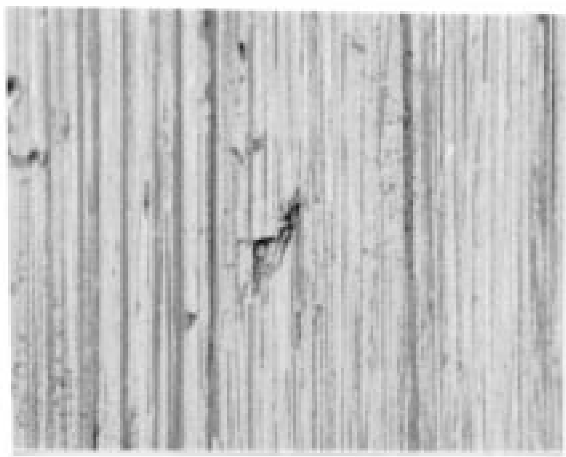

(a) CHD611, $\Delta\varepsilon_t$ = 0.62%, 10 cycles

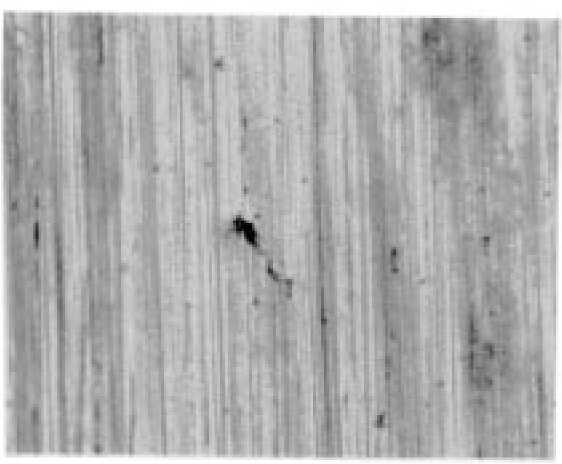

(b) CHD4, $\Delta\varepsilon_t$ = 0.62%, 10 cycles + $\Delta\varepsilon_t$ = 0.40%, 30,000 cycles

(c) CHD7, $\Delta\varepsilon_t$ = 0.40%, 30,000 cycles

Figure 7
Optical Micrographs of Sample Surface Replicas at Various Stages of Fatigue Cycling: (a) CHD611, $\Delta\varepsilon_t$ = 0.62%, 10 cycles; (b) CHD4, $\Delta\varepsilon_t$ = 0.62%, 10 cycles + $\Delta\varepsilon_t$ = 0.40%, 30,000 cycles; and (c) CHD7, $\Delta\varepsilon_t$ = 0.40%, 30,000 cycles

TEM micrographs of select samples are shown in Figures 8a–h. The cell structure originally formed in SA508 by heat treatment proved very stable, and no differences in cell structures between fatigued material and the as-received sample were observed.

(a) As received

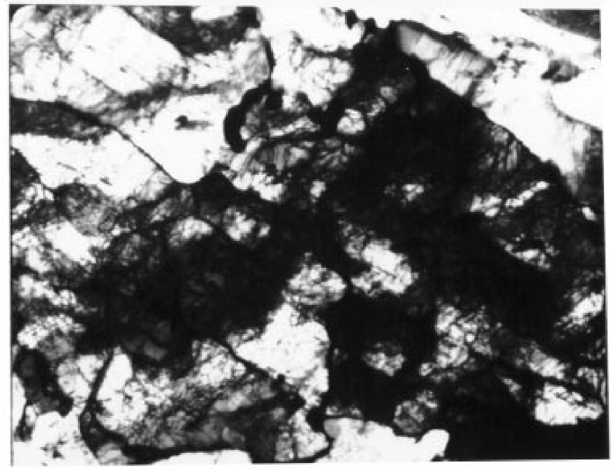

(b) CHD611, $\Delta\varepsilon_t$ = 0.62% x 10 cycles

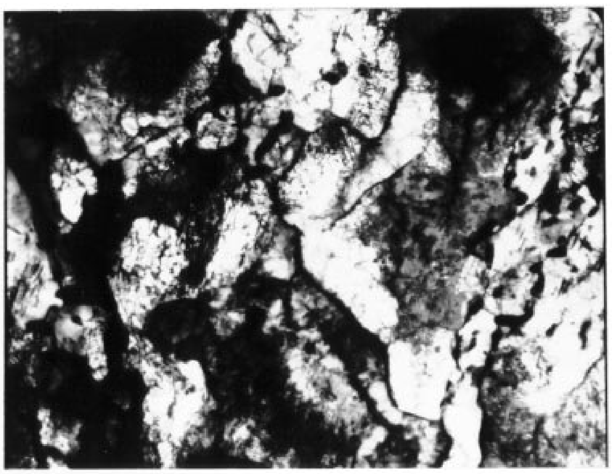

(c) CHD612, $\Delta\varepsilon_t$ = 0.62% x 10 cycles + 0.40% x 10^6

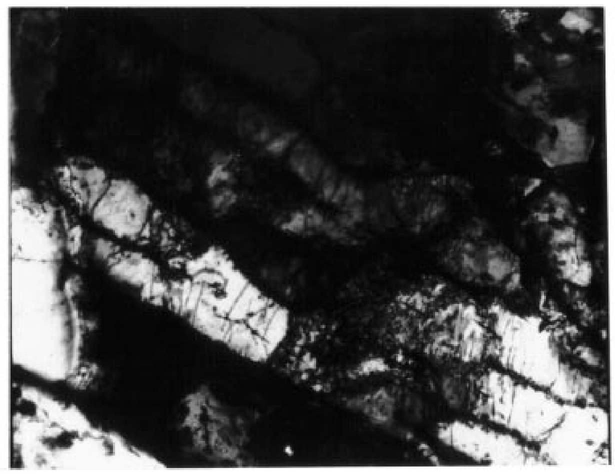

(d) CHD607, $\Delta\varepsilon_t$ = 0.62% x 10 cycles + 0.40% x 10^6 + 0.62% x 19,363 failed

1µm

Figure 8
TEM Micrographs of Samples with Different Fatigue Histories: (a) As-Received; (b) CHD611, $\Delta\varepsilon_t$ = 0.62% x 10 cycles; (c) CHD612, $\Delta\varepsilon_t$ = 0.62% x 10 cycles + 0.40% x 10^6; (d) CHD607, $\Delta\varepsilon_t$ = 0.62% x 10 cycles +0.40% x 10^6 + 0.62% x 19,363 failed

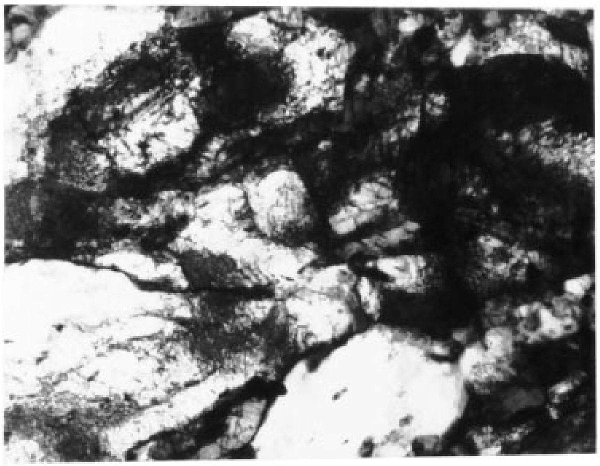

(e) CD7, $\Delta\varepsilon_t$ = 0.40% x 30,000

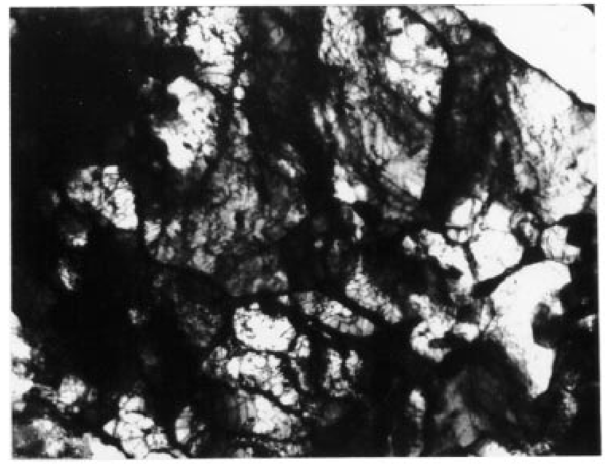

(f) CHD610, $\Delta\varepsilon_t$ = 0.62% x 100 cycles

(g) CHD6, $\Delta\varepsilon_t$ = 0.62% x 100 cycles + 0.40% x 30,000

(h) CHD605, $\Delta\varepsilon_t$ = 0.62% x 100 cycles + 0.40% x 10^6 + 0.62% x 19,225 failed

1μm

Figure 8
TEM Micrographs of Samples with Different Fatigue Histories: (e) CHD7, $\Delta\varepsilon_t$ = 0.40% x 30,000; (f) CHD610, $\Delta\varepsilon_t$ = 0.62% x 100 cycles; (g) CHD6, $\Delta\varepsilon_t$ = 0.62% x 100 cycles + 0.40% x 30,000; and (h) CHD605, $\Delta\varepsilon_t$ = 0.62% x 100 cycles + 0.40% x 10^6 + 0.62% x 9.225 failed

As shown in Table 3, the mean angular misorientation differences measured by the SAD technique for the failed samples range from 4 degrees–5 degrees. The average value of 4.3 degrees is significantly higher than the value for the as-received sample, 1.9 degrees. These findings are consistent with previous results [1,2,3,4,5].

Figure 9 shows the mean misorientation change during cycling under varying test sequences. The first stage and the third stage show the misorientation change during cycling under 0.62% total strain range, and the second stage is the misorientation change during cycling under 0.40% total strain range.

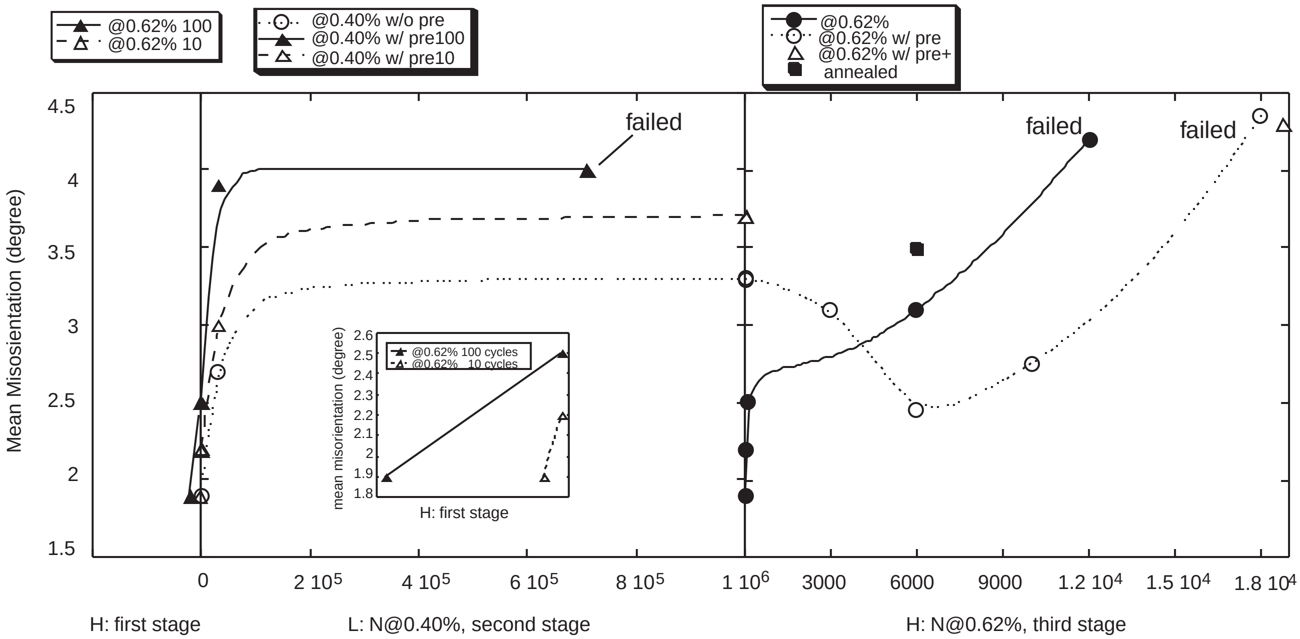

Figure 9
Mean Misorientation Change during Fatigue Life in Different Fatigue Sequences (Note: Different stages are drawn separately as first, second, and third stages.)

In the third stage of Figure 9, solid circle markers represent the misorientation change without pre-cycling and open circle markers represent the misorientation change during fatigue cycling after pre-cycling below the fatigue limit (misorientation change throughout the overall sample life is shown in the second and the third stage of Figure 9). It is interesting to note that the cell-to-cell angular misorientation increases monotonically with an increase of fatigue damage without pre-cycling, while the misorientation decreases during the early stage of the fatigue life (open circles) after pre-cycling below the fatigue limit. It is not clear why misorientation decreases after pre-cycling below the fatigue limit, but it is consistent with the fact that the samples with pre-cycling below the fatigue limit exhibit a longer lifetime than samples without pre-cycling.

The closed square marker at 6,000 cycles in the third stage of Figure 9 represents a sample pre-cycled below the fatigue limit followed by annealing at 300°C for 2.5 hours. This sample was tested to determine if the decrease in angular misorientation observed as a function of cycles occurred solely due to the test temperature. Cycling at a total strain range of 0.62% for 6,000 cycles also required approximately 2.5 hours. The angular misorientation of the annealed sample is approximately 3.5 degrees and does not show any decrease due solely to annealing temperature.

Note in the third stage of Figure 9 that angular misorientation changes quickly during the early stage of fatigue followed by a more gradual increase (closed circles). This emphasizes the importance of early stage loadings on the overall fatigue life.

The second stage of Figure 9 also demonstrates a rapid increase in angular misorientation during the early stage of fatigue cycling. However, for cycling below the fatigue endurance limit, the angular misorientation appears to saturate. The saturation of the stress depends on the pre-cycling histories (the first stage). The open circle markers represent fatigue samples without pre-cycling (second stage). Open and solid triangle markers represent samples pre-cycled above the fatigue limit for 10 cycles and 100 cycles, respectively (first stage). The angular misorientation saturation point (second stage) increases with an increase in the number of pre-cycles performed. One sample failed during cycling below the fatigue limit when the misorientation change exceeded the critical angle, 4 degrees–5 degrees. As discussed above, significant microstructural changes occur in the relatively early stages of the cycling regardless of loading amplitudes, and this early stage can significantly influence subsequent fatigue life.

In terms of microstructure, the effect of early stage cycling can be quite different from that of later cycling. To sustain the macroscopic structural changes that occur during cycling, geometrically necessary dislocations are introduced in the sample [18]. The relationship between loading direction and activated slip systems varies among grain to grain. Thus, in order to sustain the continuity of grain boundaries, geometrically necessary dislocations are induced at the beginning of the cycling. When subsequent cycling is performed, to-and-fro motion of the dislocations already induced can sustain the cycling. If the loading is changed to a higher amplitude, other slip systems can also be activated whose dislocations had not moved at the previous lower level of stress. When the loading is changed to a lower amplitude from a higher amplitude, these slip systems might stop working. Thus, the low-to-high loading and the high-to-low loading sequences can be quite different microstructurally, and even a small amount of cycling may significantly influence the lifetime. Evidence of this can be seen in Figure 9. Microstructural behavior during the higher loading level (third stage) preceded by pre-cycling at the lower loading level (second stage) exhibits inflection points, while only a monotonic increase of the misorientation change is observed during lower loading (second stage) after pre-cycling at the higher loading level (first stage). It is not yet understood why cell-to-cell misorientation decreases when the specimens are subjected to low-to-high loading. Further study is necessary to clarify this phenomenon.

As previously discussed, the fatigue samples that failed exhibited an angular misorientation value of approximately 4 degrees–5 degrees. This suggests a critical misorientation value that can be used in a future screening methodology for assessment of plant component fatigue. For fatigue testing below the endurance limit (0.40% strain range for SA508), an angular misorientation value of 3.3 degrees was obtained even after testing to 1×10^6 cycles without sample failure. The SAD technique can be used to measure microstructural changes in a material and confirm the endurance limit value.

These observations suggest that the SAD technique can also provide valuable information regarding the impact of reactor water environment on component fatigue life. Investigations to date have focused on performing fatigue tests under specific environmental conditions to determine the impact on component fatigue life. Further study utilizing the SAD technique is warranted to measure the microstructural changes in samples exposed to reactor water environments in order to correlate angular misorientation with a reduction in fatigue life due to environmental factors. This can ultimately lead to an approach to monitor inservice components and determine when, or if, a reduction in fatigue life might be approaching a value where component repair or replacement is necessary. In addition, data from SAD measurements can help verify the impact of reactor water environment on material fatigue life and establish a threshold value for component life assessment.

6

FEASIBILITY STUDY FOR EBSP

Overview of Electron Backscattering Diffraction Patterns (EBSP)

When a focused electron beam enters into a crystalline material, a percentage of the incident electrons will disperse beneath the material's surface and diffract. This diffraction will cause the electrons to lose energy and no longer interact with the incident beam. As diffraction occurs in all directions, angles exist which satisfy Bragg's condition for crystallographic planes. For each set of crystal planes in a sample, two distinct electron path "cones" exist, which are directed away from either side of the crystal planes as shown in Figure 10. These diffracted electrons are referred to as backscattered Kikuchi diffraction patterns (BKD patterns), or electron backscattering diffraction patterns (EBSP) [15].

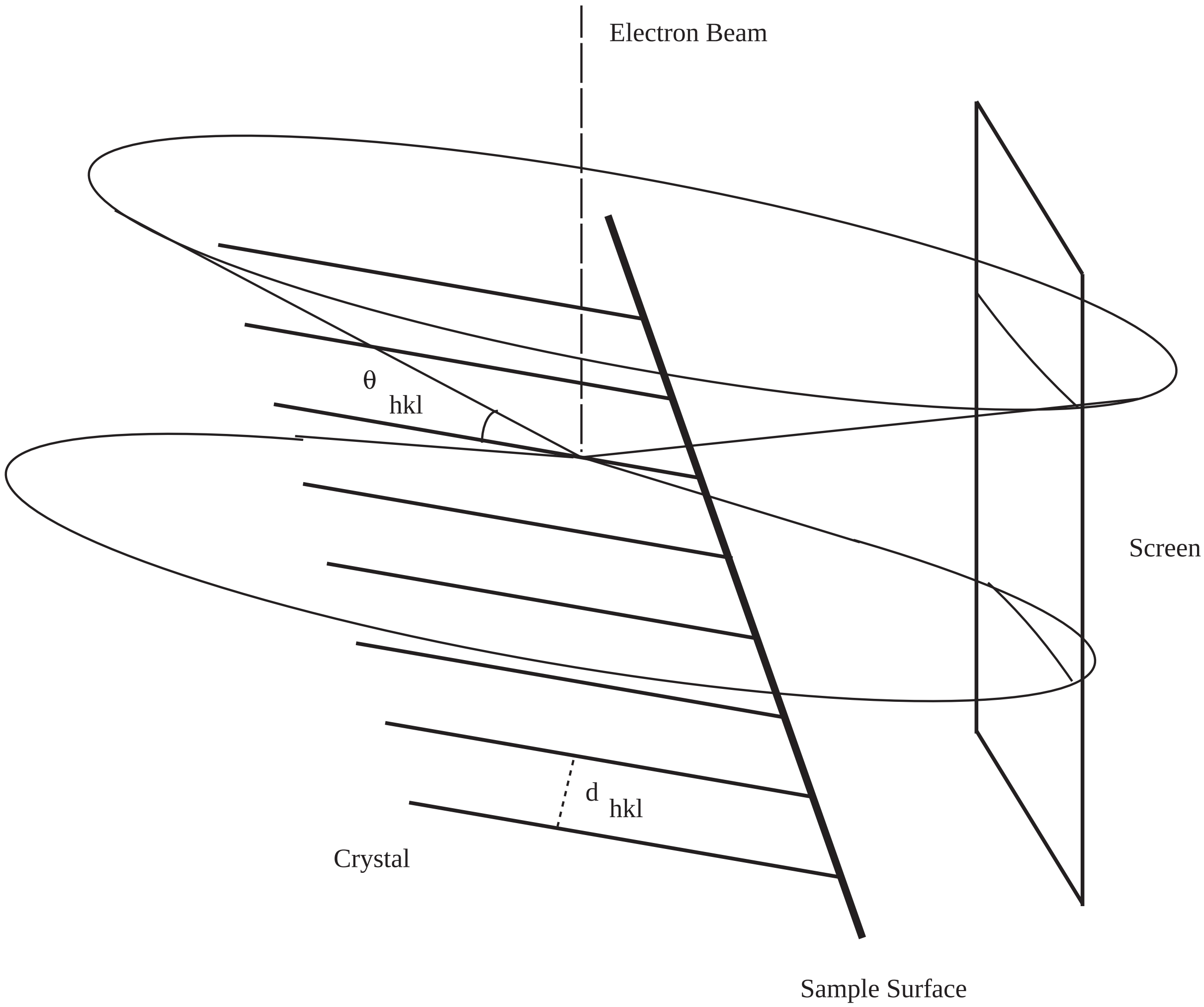

Figure 10
Generation of EBSP by Channeling of Low-Loss Electrons along Crystal Planes

Detection of EBSP

EBSP can be detected by placing a phosphor screen close to the sample as illustrated in Figures 10 and 11. Note that the sample is inclined towards the screen. Care should be exercised regarding placement of the screen in proximity to the sample. At long distances, the total number of electrons involved in formation of the pattern is low; hence, the signal-to-noise ratio is low. In addition, for a fixed phosphor screen diameter, the number of poles that can be detected decreases with increasing distance. In other words, at long distances only a portion of the pattern is visible. Alternatively, too short a distance will risk sample contact with the phosphor screen. In this study, the phosphor screen was maintained at a distance of 50 mm from the sample. This distance was automatically established by the TSL OIM system installed on the SEM.

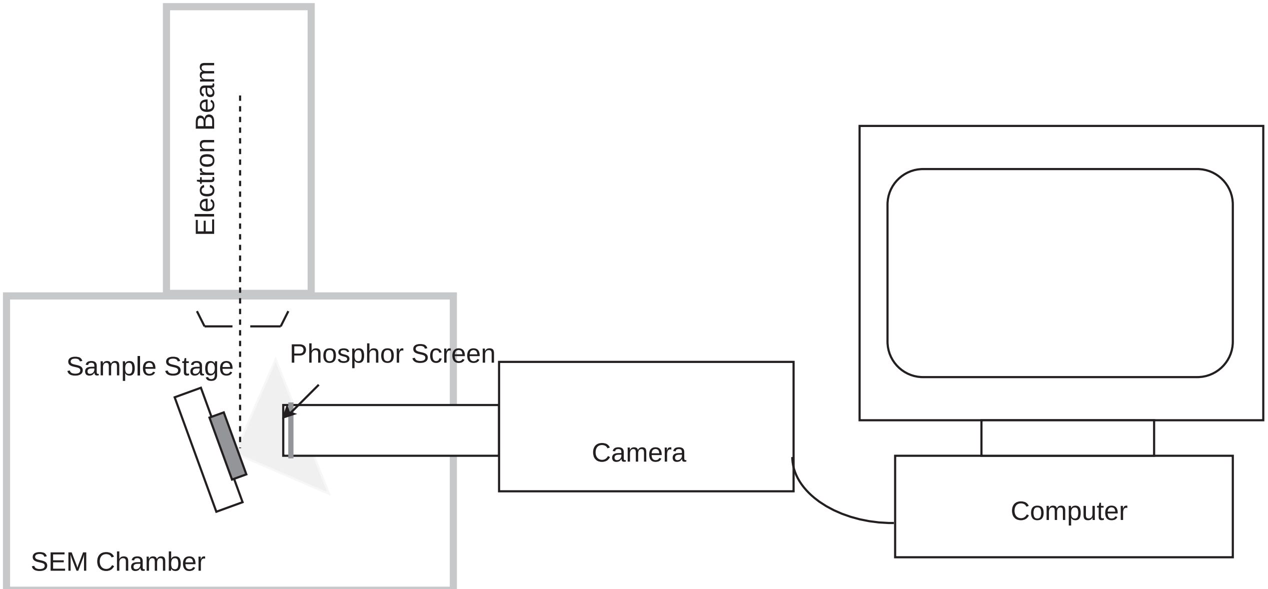

Figure 11
Schematic Set-up for Detection of EBSP

Characteristics of EBSP

A large amount of information regarding the local structure of a material is available through EBSP. Specifically, precise lattice orientation information can be obtained. Figure 12 illustrates an example of EBSP taken from an SA508 sample. The pattern consists of several pairs of parallel lines that intersect at various places. Each pair of lines, known as Kikuchi lines, represent a specific plane orientation in the crystal, and the spacing between line pairs is inversely proportional to the interplanar spacing. The intersection points of individual Kikuchi lines represent crystallographic directions. It has been previously established that local orientation information can be obtained by EBSP, but indexing the pattern to crystallographic orientation requires considerable skill in crystallography. Recently, automated indexing software has been developed that provides for statistical data processing [13,14].

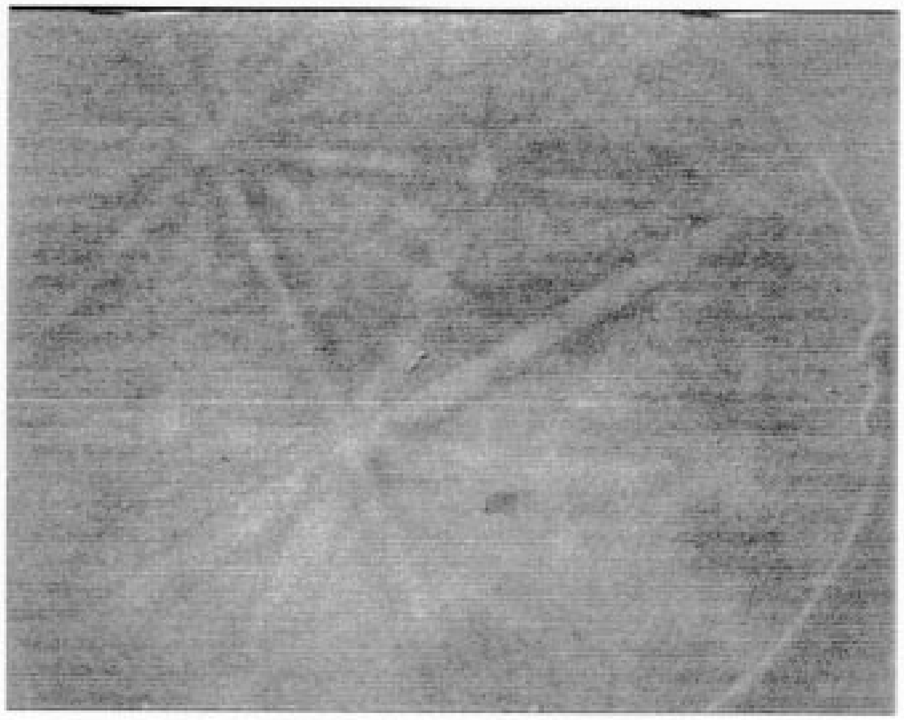

(a) Electron backscattered Kikuchi driffraction pattern obtained from sample.

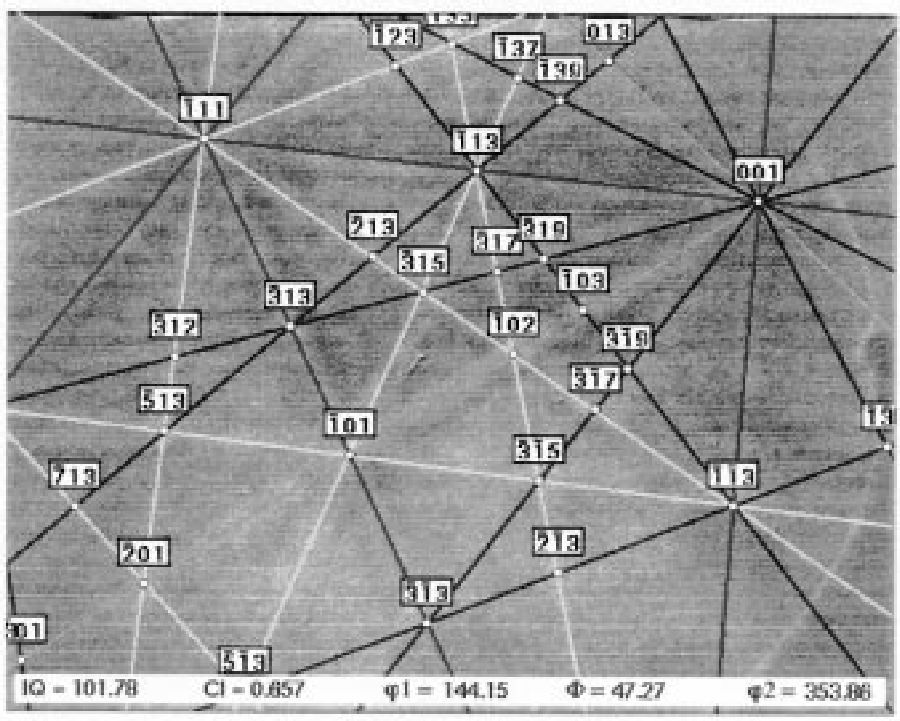

(b) Indexed diffraction pattern.

Figure 12
EBSP Image Obtained from SA508: (a) Electron Backscattered Kikuchi Diffraction Pattern Obtained from Sample and (b) Indexed Diffraction Pattern. See color version on page 6-13.

Results and Discussion

The EBSP technique was applied to as-received, 0.08%, 0.8%, 10%, 25%, 50%, and 100% fatigued SA508 samples. EBSP images were successfully obtained from the SA508 samples. Examples of orientation imagings of SA508 samples obtained through the EBSP technique are shown in Figures 13a–c. The planar misorientation determined through analysis of EBSP data are illustrated according to the following scheme:

1. q ≥ 15 degrees minimum misorientation (black lines)
2. 15 > q ≥ 5 degrees misorientation (blue lines)
3. 5 > q ≥ 1 degree misorientation (green lines)
4. 1 > q ≥ 0.5 degrees misorientation (red lines)

These mappings represent similar microstructural areas as shown in Figure 8. No significant increase in the planar misorientation is apparent in Figures 13a–c as fatigue damage increased.

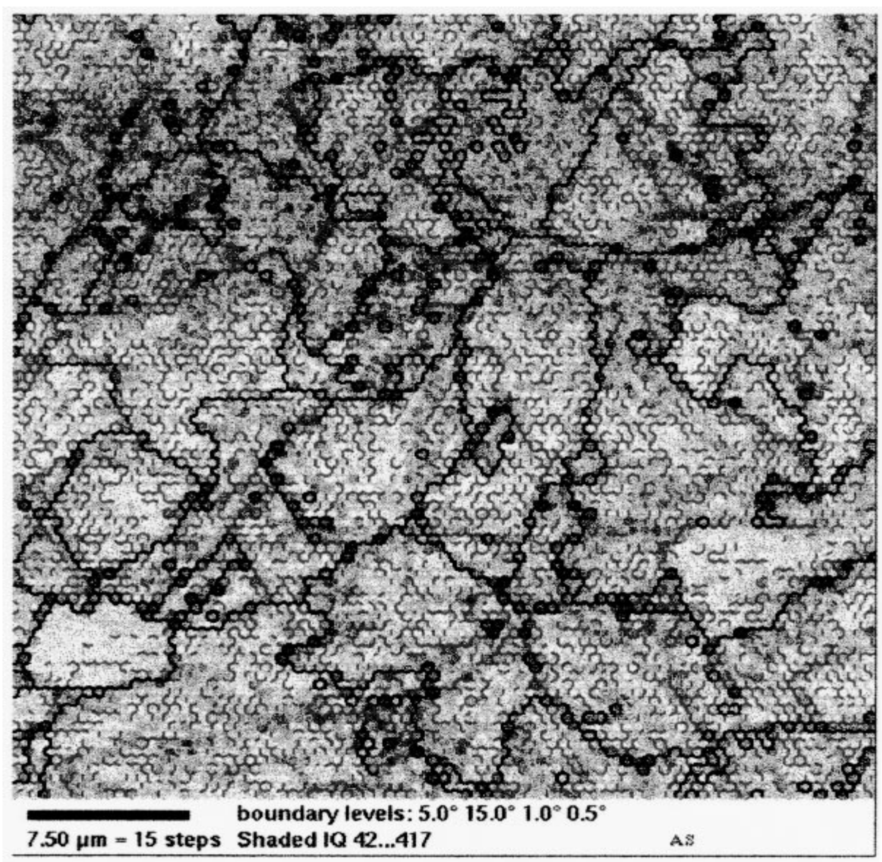

Note: 0.5-1 deg. red, 1-5 deg. green, 5-15 deg. blue, 15 deg.< black

(a) As-received

Figure 13a
Orientation Imagings of SSA508, As-Received. See color version on page 6-14.

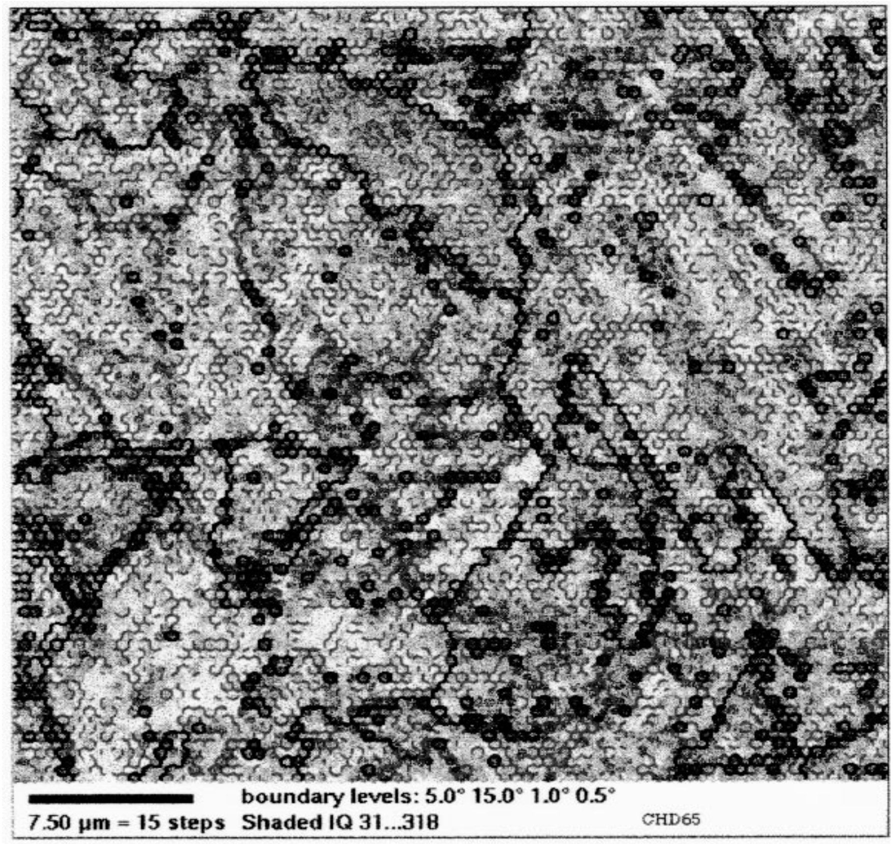

Note: 0.5-1 deg. red, 1-5 deg. green, 5-15 deg. blue, 15 deg.< black

(b) CHD65: N/N = 50%, $\Delta\varepsilon_t = 0.62\%$

Figure 13b
Orientation Imagings of SSA508, CHD65: N/N = 50%, $\Delta\varepsilon_t$ = 0.62%. See color version on page 6-15.

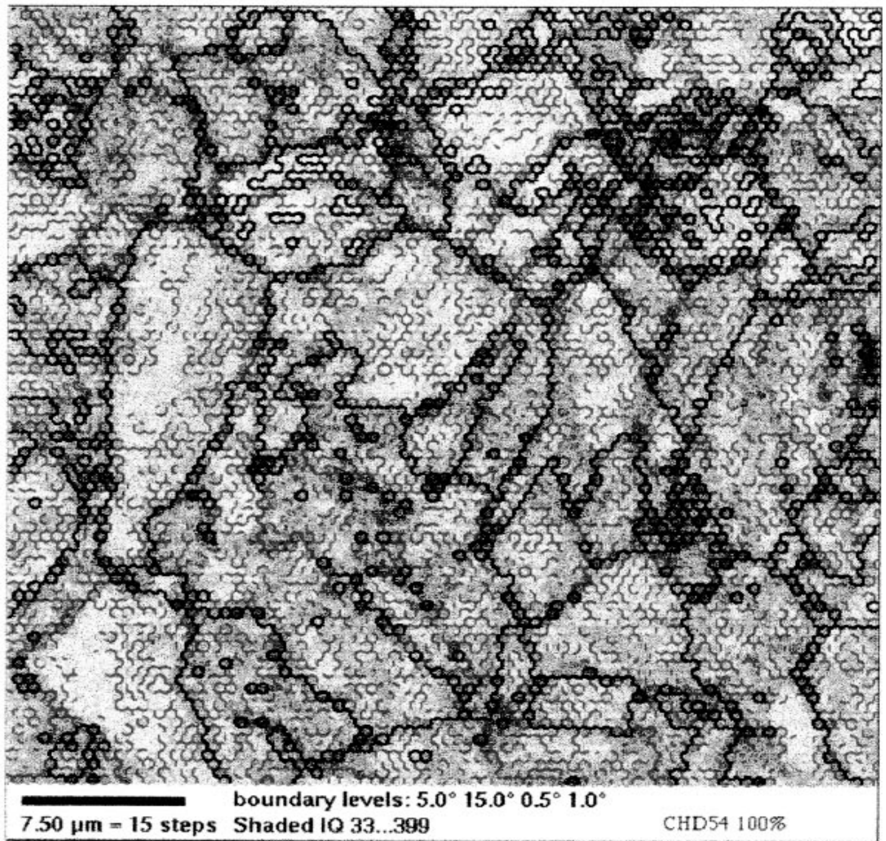

Note: 0.5-1 deg. red, 1-5 deg. green, 5-15 deg. blue, 15 deg.< black

(c) CHD54: N/N = 100%, $\Delta\varepsilon_t = 0.62\%$

Figure 13c
Orientation Imagings of SSA508, CHD54: N/N$_t$ =100%, $\Delta\varepsilon_t$ = 0.62%. See color version on page 6-16.

Misorientation histograms for SA508 are shown in Figures 14a–c. A majority of the misorientation shown occurred below a value of 4 degrees. However, no apparent difference in misorientation below 4 degrees can be distinguished between the fatigued and as-received samples.

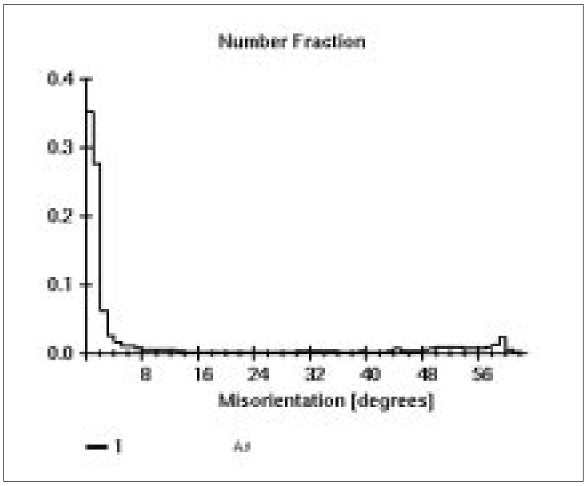

(a) As-Received

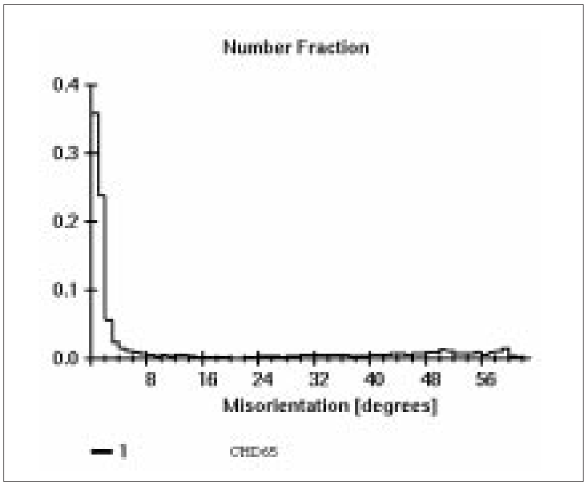

(b) 50%

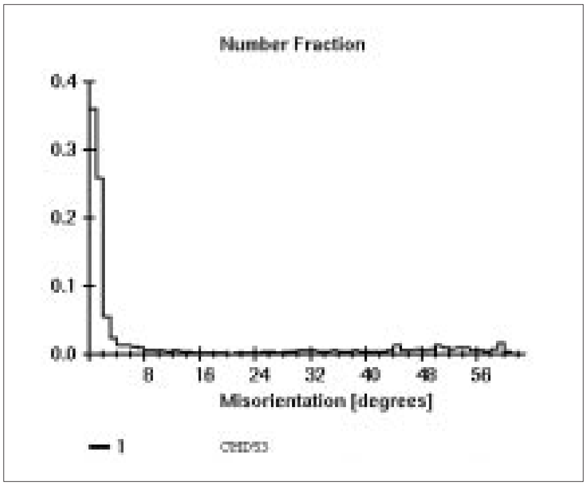

(c) 100%

Figure 14
Misorientation Histograms for SA508: (a) As-Received, (b) 50%, and (c) 100%

Figure 15 shows the normal distribution plots of angular misorientation within grains as measured with the EBSP technique. Each datum represents misorientation measured by the following procedure:

1. The interfaces with q ≥ 15 degrees minimum misorientation and with 15 > q ≥ 5 degrees misorientation were highlighted.
2. A point was defined as a central point of a grain.
3. The misorientation was measured between the central defined point and a second, randomly selected point within a grain. This process was performed a total of 6 times for each grain selected.

Examples of the misorientation measurements performed are shown in Figures 16a–d and indicated by colored markers.

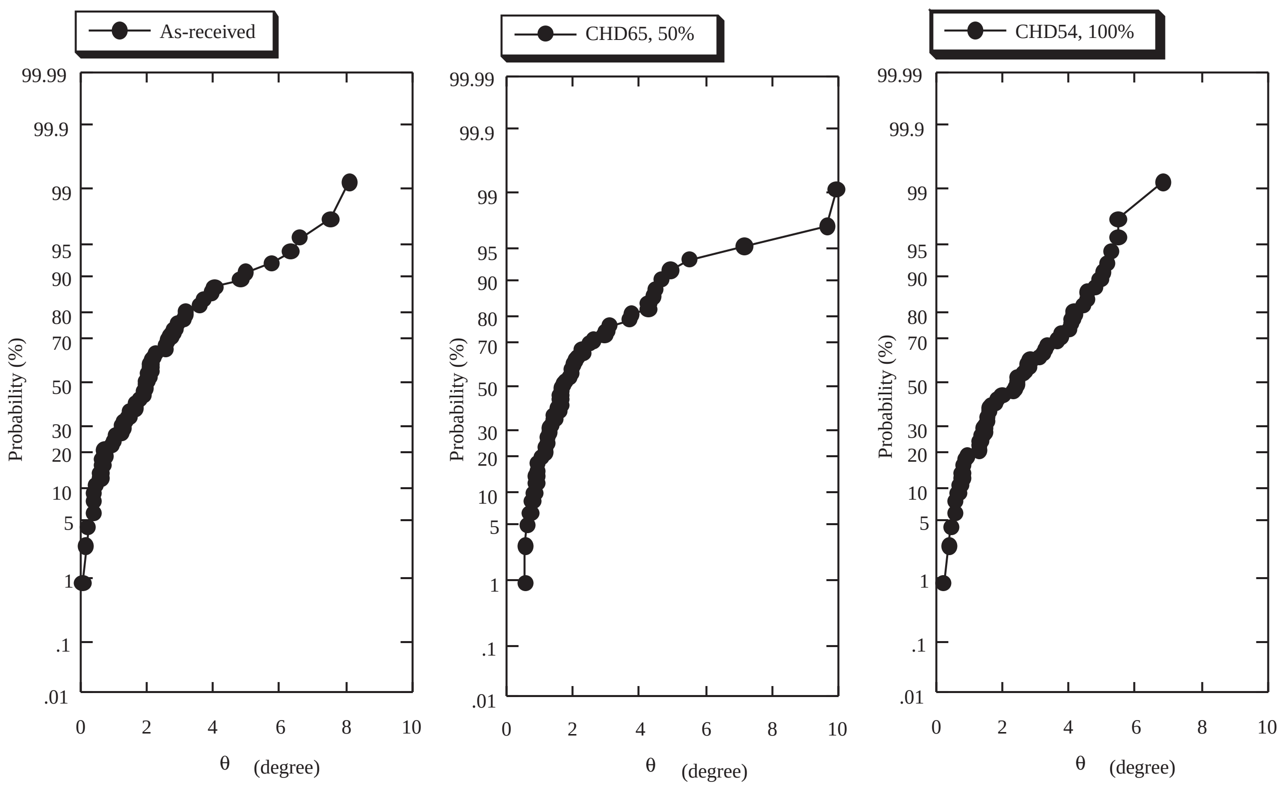

Figure 15
Normal Distribution Plots of Misorientation within Grains Measured by EBSP

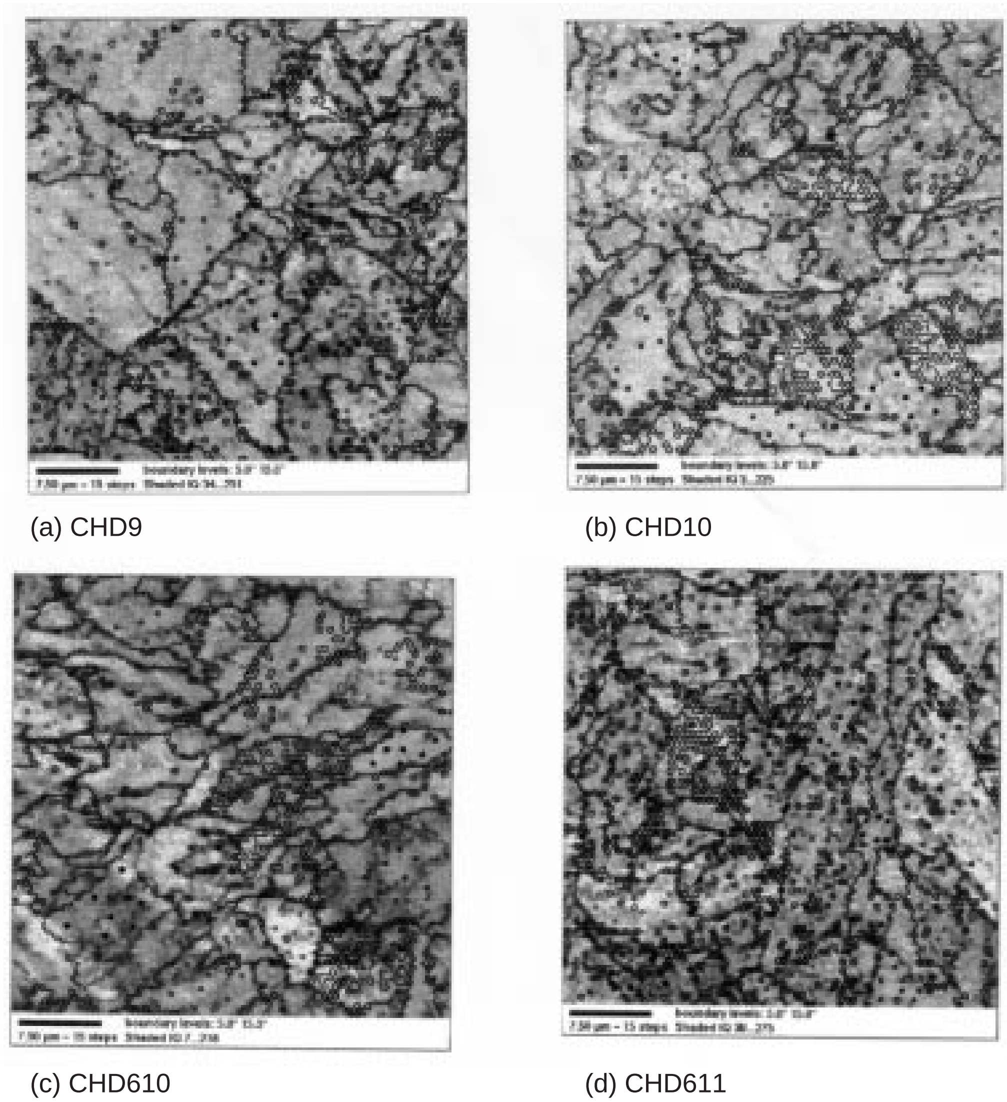

Figure 16
EBSP Misorientation Measurement Locations: (a) CHD9, (b) CHD10, (c) CHD610, and (d) CHD611. See color version on page 6-17.

A comparison of the normal distribution plots obtained through EBSP (Figure 15) with those obtained through SAD (Figures 4a–c) indicates a distinct difference between results from the two approaches. The SAD results are scattered around a linear trend in the normal distribution plots. Note that the slope of the curve (which is inversely proportional to the standard deviation) decreases with an increase in fatigue damage. The EBSP results do not exhibit linear behavior on the normal distribution plots and do not reveal a clear relationship with fatigue damage.

The mean misorientation of ten grains (the average of 10 grains with 6 measurements per grain) measured by EBSP are plotted as a function of fatigue damage accumulation in Figure 17. In general, the trend is similar to the SAD results, except for the data representing 10% and 25% cumulative fatigue damage. Note that the misorientation change measured by EBSP is much smaller than the change measured by SAD. It is not clear at this time if the small changes observed by EBSP are physically based changes that can be correlated with accumulated fatigue damage or are simply artifacts of data scatter.

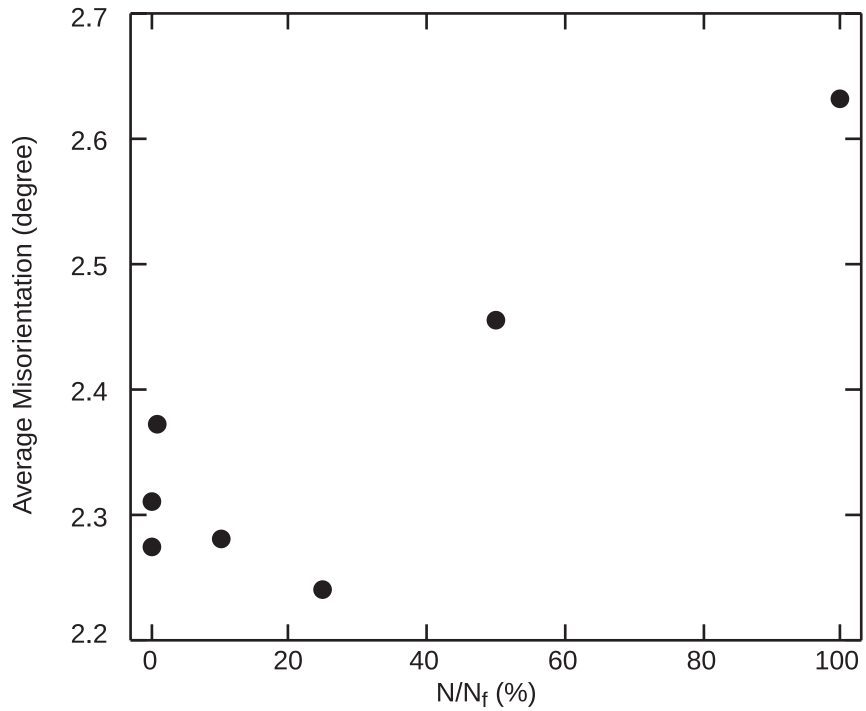

Figure 17
Mean Misorientation Change during Fatigue Measured by EBSP

The SAD and the EBSP techniques appear to yield markedly different results. Differences exist between the EBSP and the SAD measurement techniques that might provide insight. During SAD measurements, the diffraction patterns can be optically observed. In this study, SAD measurements have been performed so that the largest misorientation is recorded on film. The SAD technique measures misorientation between cell substructures within individual grains. As dislocation motion occurs during fatigue, misorientation will occur within the cell substructure. In other words, misorientation between cells increases with the increase of fatigue damage. Cell-to-cell misorientation will increase, but the overall distortion must be accommodated within each grain. No long range order misorientation change should exist within a grain. For example, if misorientation at one cell boundary is 5 degrees, the misorientation at the other side of this cell should be -5 degrees, on average. (Misorientation does not have to be compensated within a cell, but it must be compensated within a grain.) The SAD technique is well suited to detect the largest misorientation within a grain.

In contrast to the SAD technique, EBSP measurements might not always reflect the largest cell-to-cell misorientation. The six EBSP measurements taken within each grain are performed at locations automatically selected at random. As prior TEM observation to determine the largest misorientation was not performed, the cell-to-cell misorientation measured will likely not be the maximum value. However, additional statistical analysis can likely resolve this issue. In addition, the SAD technique measures misorientation around the <111> direction between cells, in two-dimensional space. Misorientation change during fatigue may vary with crystallographic direction and stress axis. Therefore, the same orientation axis should be used to provide a consistent basis for comparison.

The EBSP technique measures misorientation around an arbitrary direction between cells, in three-dimensional space. Thus, the axis around which measurements are taken is always the eigenvector for the transformation between the two measurement points.

Further investigation and analysis is required to clarify the phenomenon.

7

CONCLUSIONS

Fatigue test bars fabricated from an SA508 steel plate were cyclically deformed under different loading regimes to investigate the influence of loading sequences on the fatigue life, with special consideration given to the early stages of cycling. Specimens were subjected to high-to-low and low-to-high amplitude cyclic strain, including both below (total strain range of 0.40%) and above (total strain range of 0.62%) the fatigue limit. High-to-low loadings initially included 10 cycles and 100 cycles of high strain range loadings. These small numbers of cycles were less than 1% of the total lifetime when the specimens were subjected to the constant amplitude fatigue test. Specimens were then cut perpendicular to the stress axis within the gage section at a minimum distance of 5 mm from any observable cracks. TEM microscopy was utilized to obtain microstructural characteristics of the samples, and cell-to-cell angular misorientation differences were measured by the SAD method. Surface cracking was also observed by the surface replication technique.

The EBSP technique was applied to specimens previously measured using the SAD technique in order to compare results and evaluate application of the two techniques. Crystallographic orientation data were analyzed to determine the feasibility of this technique for measuring the state of fatigue damage accumulation. The results were compared with the SAD measurements previously performed on the same material to determine the preferred method for quantitatively measuring fatigue damage. EBSP images were obtained from the SA508 specimens, even though the material had well developed cell structures and a high dislocation density. The orientation imagings drawn from the EBSP data were similar to observed TEM images.

The following conclusions are drawn from the Phase I activities described:

1. The average cell-to-cell misorientation increases with fatigue damage accumulation. This phenomenon was observed even during cycling below the fatigue limit.
2. The specimens pre-cycled below the fatigue limit or pre-cycled above the fatigue limit for 10 cycles followed by additional pre-cycling below the fatigue limit showed an increase in fatigue lifetime of about 50% from the original lifetime, when subsequent cycling was carried out at a total strain range above the fatigue limit. In contrast, specimens that were pre-cycled above the fatigue limit for 6,000 cycles, or even 100 cycles, subsequently failed even when cycled below the fatigue limit.

3. The cell-to-cell misorientation differences measured via the SAD technique were shown to decrease during cycling above the fatigue limit after initial pre-cycling below the fatigue limit. This is consistent with the fact that fatigue lifetime is enhanced by pre-cycling below the fatigue limit.
4. Small cracks were observed after pre-cycling both below and above the fatigue limit. Several specimens exhibited extended life with small surface cracks, and the life was affected by the loading sequence.
5. The misorientation histograms obtained from the EBSP measurements showed no significant differences between fatigued and as-received samples.
6. The misorientation within a grain was measured via EBSP for ten grains for each sample and the average misorientation of the sample obtained. The average misorientation slightly increased with an increase in fatigue damage. The misorientation change measured by EBSP was much smaller than that measured by SAD.
7. The EBSP method may be feasible to measure microstructural changes during fatigue, if improved data processing is performed. Based on the results of this study, however, it appears that EBSP will not reduce the inspection time and cost as compared to the SAD technique.

8

BIBLIOGRAPHY

1. Fukuoka, C., Nakagawa, Y.G., Lance, J.J., and Pangborn, R.N., Metall. Trans. A, 1996, vol. 27A, pp. 3841-51.
2. Nakagawa, Y.G., Yoshizawa, H., and Lapides, M.E., Metall. Trans. A, 1990, vol. 21A, pp. 1769-73.
3. Fukuoka, C., Yoshizawa, H., Nakagawa, Y.G., and Lapides, M.E., Metall. Trans. A, 1993, vol. 24A, pp. 2209-16.
4. Lapides, M.E., Nakagawa, Y.G., Fukuoka, C., and Yoshida, Y., 1994 "ASME Pressure Vessels and Piping Conference," Minneapolis, MN, PVP-vol. 283, pp. 23-28.
5. Fukuoka, C. and Nakagawa, Y.G., Scripta Metallurgica, 1996, vol. 34, No. 9, pp. 1497-1502.
6. Bennett, J.A., Proc. Amer. Soc. Test. Mat., vol. 46, 1946, p. 693
7. Richart, F.E. and Newmark, N.M., Proc. Amer. Soc. Test. Mat., vol. 48, 1948, p. 767.
8. Marco, S.M. and Starkey, W.L., Trans. Amer. Soc. Mech. Engrs., vol. 76, 1954, p. 627.
9. Goto, M., Nisitani, H., Yanagawa, Y., and Miyagawa, H., Nihon Kikaigakkai ronbunshyu, A., vol. 55, no. 511, 1989, pp. 453-459.
10. Sinclair, G.M., Proc. ASTM, 1952, vol. 52, pp. 743-758.
11. Nisitani, H. and Ikenaga, T., Kikai no Kenkyuu (Research in Mechanics), vol. 27, no. 8, 1975, pp. 995-1000.
12. Fleck, N.A., Acta Metallurgica, vol. 33, 1985, pp. 1339-54.
13. Adams, B.L., Wright, S.I., and Kunze, K., Metall. Trans. A, vol. 24A, 1993, pp. 819-831.
14. Day, A. and Shafirstein, G., Materials Science and Technology, vol. 12, 1996, pp. 873-879.
15. Blackham, M.N., Alam, M., and Pashlay, D.W., Proc. R. Soc. London, 1953, vol. A221, pp. 224-42.
16. Miller, K.J., *Fundamentals of Deformation and Fracture, Eshelby Memorial Symposium Sheffield, April 2-5 1984*, ed. B.A. Bilby, K.J. Miller, and J.R. Willis, pp. 477-499.

17. Miller, K.J., Fatigue of Engineering Materials and Structures, vol. 5, no. 3, 1982, pp. 223-232.

18. Ashby, M. F., Philosophical Magazine, vol. 21, 1970, pp. 399-424.

WARNING: This Document contains information classified under U.S. Export Control regulations as restricted from export outside the United States. You are under an obligation to ensure that you have a legal right to obtain access to this information and to ensure that you obtain an export license prior to any re-export of this information. Special restrictions apply to access by anyone that is not a United States citizen or a Permanent United States resident. For further information regarding your obligations, please see the information contained below in the section titled "Export Control Restrictions."

Export Control Restrictions

Access to and use of EPRI Intellectual Property is granted with the specific understanding and requirement that responsibility for ensuring full compliance with all applicable U.S. and foreign export laws and regulations is being undertaken by you and your company. This includes an obligation to ensure that any individual receiving access hereunder who is not a U.S. citizen or permanent U.S. resident is permitted access under applicable U.S. and foreign export laws and regulations. In the event you are uncertain whether you or your company may lawfully obtain access to this EPRI Intellectual Property, you acknowledge that it is your obligation to consult with your company's legal counsel to determine whether this access is lawful. Although EPRI may make available on a case by case basis an informal assessment of the applicable U.S. export classification for specific EPRI Intellectual Property, you and your company acknowledge that this assessment is solely for informational purposes and not for reliance purposes. You and your company acknowledge that it is still the obligation of you and your company to make your own assessment of the applicable U.S. export classification and ensure compliance accordingly. You and your company understand and acknowledge your obligations to make a prompt report to EPRI and the appropriate authorities regarding any access to or use of EPRI Intellectual Property hereunder that may be in violation of applicable U.S. or foreign export laws or regulations.

About EPRI

EPRI creates science and technology solutions for the global energy and energy services industry. U.S. electric utilities established the Electric Power Research Institute in 1973 as a nonprofit research consortium for the benefit of utility members, their customers, and society. Now known simply as EPRI, the company provides a wide range of innovative products and services to more than 1000 energy-related organizations in 40 countries. EPRI's multidisciplinary team of scientists and engineers draws on a worldwide network of technical and business expertise to help solve today's toughest energy and environmental problems.

EPRI. Electrify the World

SINGLE USER LICENSE AGREEMENT

THIS IS A LEGALLY BINDING AGREEMENT BETWEEN YOU AND THE ELECTRIC POWER RESEARCH INSTITUTE, INC. (EPRI). PLEASE READ IT CAREFULLY BEFORE REMOVING THE WRAPPING MATERIAL.

BY OPENING THIS SEALED PACKAGE YOU ARE AGREEING TO THE TERMS OF THIS AGREEMENT. IF YOU DO NOT AGREE TO THE TERMS OF THIS AGREEMENT, PROMPTLY RETURN THE UNOPENED PACKAGE TO EPRI AND THE PURCHASE PRICE WILL BE REFUNDED.

1. GRANT OF LICENSE

EPRI grants you the nonexclusive and nontransferable right during the term of this agreement to use this package only for your own benefit and the benefit of your organization. This means that the following may use this package: (I) your company (at any site owned or operated by your company); (II) its subsidiaries or other related entities; and (III) a consultant to your company or related entities, if the consultant has entered into a contract agreeing not to disclose the package outside of its organization or to use the package for its own benefit or the benefit of any party other than your company.

This shrink-wrap license agreement is subordinate to the terms of the Master Utility License Agreement between most U.S. EPRI member utilities and EPRI. Any EPRI member utility that does not have a Master Utility License Agreement may get one on request.

2. COPYRIGHT

This package, including the information contained in it, is either licensed to EPRI or owned by EPRI and is protected by United States and international copyright laws. You may not, without the prior written permission of EPRI, reproduce, translate or modify this package, in any form, in whole or in part, or prepare any derivative work based on this package.

3. RESTRICTIONS

You may not rent, lease, license, disclose or give this package to any person or organization, or use the information contained in this package, for the benefit of any third party or for any purpose other than as specified above unless such use is with the prior written permission of EPRI. You agree to take all reasonable steps to prevent unauthorized disclosure or use of this package. Except as specified above, this agreement does not grant you any right to patents, copyrights, trade secrets, trade names, trademarks or any other intellectual property, rights or licenses in respect of this package.

4. TERM AND TERMINATION

This license and this agreement are effective until terminated. You may terminate them at any time by destroying this package. EPRI has the right to terminate the license and this agreement immediately if you fail to comply with any term or condition of this agreement. Upon any termination you may destroy this package, but all obligations of nondisclosure will remain in effect.

5. DISCLAIMER OF WARRANTIES AND LIMITATION OF LIABILITIES

NEITHER EPRI, ANY MEMBER OF EPRI, ANY COSPONSOR, NOR ANY PERSON OR ORGANIZATION ACTING ON BEHALF OF ANY OF THEM:

(A) MAKES ANY WARRANTY OR REPRESENTATION WHATSOEVER, EXPRESS OR IMPLIED, (I) WITH RESPECT TO THE USE OF ANY INFORMATION, APPARATUS, METHOD, PROCESS OR SIMILAR ITEM DISCLOSED IN THIS PACKAGE, INCLUDING MERCHANTABILITY AND FITNESS FOR A PARTICULAR PURPOSE, OR (II) THAT SUCH USE DOES NOT INFRINGE ON OR INTERFERE WITH PRIVATELY OWNED RIGHTS, INCLUDING ANY PARTY'S INTELLECTUAL PROPERTY, OR (III) THAT THIS PACKAGE IS SUITABLE TO ANY PARTICULAR USER'S CIRCUMSTANCE; OR

(B) ASSUMES RESPONSIBILITY FOR ANY DAMAGES OR OTHER LIABILITY WHATSOEVER (INCLUDING ANY CONSEQUENTIAL DAMAGES, EVEN IF EPRI OR ANY EPRI REPRESENTATIVE HAS BEEN ADVISED OF THE POSSIBILITY OF SUCH DAMAGES) RESULTING FROM YOUR SELECTION OR USE OF THIS PACKAGE OR ANY INFORMATION, APPARATUS, METHOD, PROCESS OR SIMILAR ITEM DISCLOSED IN THIS PACKAGE.

6. EXPORT

The laws and regulations of the United States restrict the export and re-export of any portion of this package, and you agree not to export or re-export this package or any related technical data in any form without the appropriate United States and foreign government approvals.

7. CHOICE OF LAW

This agreement will be governed by the laws of the State of California as applied to transactions taking place entirely in California between California residents.

8. INTEGRATION

You have read and understand this agreement, and acknowledge that it is the final, complete and exclusive agreement between you and EPRI concerning its subject matter, superseding any prior related understanding or agreement. No waiver, variation or different terms of this agreement will be enforceable against EPRI unless EPRI gives its prior written consent, signed by an officer of EPRI.

Program: TR-110250

Nuclear Power

© 1998 Electric Power Research Institute (EPRI), Inc. All rights reserved. Electric Power Research Institute and EPRI are registered service marks of the Electric Power Research Institute, Inc.
EPRI. ELECTRIFY THE WORLD is a service mark of the Electric Power Research Institute, Inc.

Printed on recycled paper in the United States of America

EPRI • 3412 Hillview Avenue, Palo Alto, California 94304 • PO Box 10412, Palo Alto, California 94303 • USA
800.313.3774 • 650.855.2121 • askepri@epri.com • www.epri.com